



This is a repository copy of *Review of zirconolite crystal chemistry and aqueous durability*.

White Rose Research Online URL for this paper:  
<https://eprints.whiterose.ac.uk/174554/>

Version: Published Version

---

**Article:**

Blackburn, L.R. [orcid.org/0000-0002-5889-2035](https://orcid.org/0000-0002-5889-2035), Bailey, D.J. [orcid.org/0000-0002-0313-8748](https://orcid.org/0000-0002-0313-8748), Sun, S.K. et al. (4 more authors) (2021) Review of zirconolite crystal chemistry and aqueous durability. *Advances in Applied Ceramics*, 120 (2). pp. 69-83. ISSN 1743-6753

<https://doi.org/10.1080/17436753.2021.1877596>

---

**Reuse**

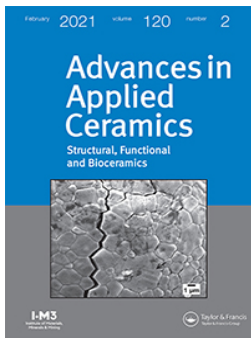
This article is distributed under the terms of the Creative Commons Attribution-NonCommercial-NoDerivs (CC BY-NC-ND) licence. This licence only allows you to download this work and share it with others as long as you credit the authors, but you can't change the article in any way or use it commercially. More information and the full terms of the licence here: <https://creativecommons.org/licenses/>

**Takedown**

If you consider content in White Rose Research Online to be in breach of UK law, please notify us by emailing [eprints@whiterose.ac.uk](mailto:eprints@whiterose.ac.uk) including the URL of the record and the reason for the withdrawal request.



[eprints@whiterose.ac.uk](mailto:eprints@whiterose.ac.uk)  
<https://eprints.whiterose.ac.uk/>



# Advances in Applied Ceramics

## Structural, Functional and Bioceramics

ISSN: (Print) (Online) Journal homepage: <https://www.tandfonline.com/loi/yaac20>

## Review of zirconolite crystal chemistry and aqueous durability

Lewis R. Blackburn, Daniel J. Bailey, Shi-Kuan Sun, Laura J. Gardner, Martin C. Stennett, Claire L. Corkhill & Neil C. Hyatt

To cite this article: Lewis R. Blackburn, Daniel J. Bailey, Shi-Kuan Sun, Laura J. Gardner, Martin C. Stennett, Claire L. Corkhill & Neil C. Hyatt (2021) Review of zirconolite crystal chemistry and aqueous durability, *Advances in Applied Ceramics*, 120:2, 69-83, DOI: [10.1080/17436753.2021.1877596](https://doi.org/10.1080/17436753.2021.1877596)

To link to this article: <https://doi.org/10.1080/17436753.2021.1877596>



© 2021 The Author(s). Published by Informa UK Limited, trading as Taylor & Francis Group



Published online: 05 May 2021.



Submit your article to this journal [↗](#)



Article views: 48






View related articles [↗](#)



View Crossmark data [↗](#)

## Review of zirconolite crystal chemistry and aqueous durability

Lewis R. Blackburn , Daniel J. Bailey, Shi-Kuan Sun, Laura J. Gardner , Martin C. Stennett, Claire L. Corkhill and Neil C. Hyatt 

Immobilisation Science Laboratory, Department of Materials Science and Engineering, University of Sheffield, Sheffield, UK

### ABSTRACT

Zirconolite ( $\text{CaZrTi}_2\text{O}_7$ ) has been identified as a candidate ceramic wasteform for the immobilisation and disposal of Pu inventories, for which there is no foreseen future use. Here, we provide an overview of relevant zirconolite solid solution chemistry with respect to Ce, U and Pu incorporation, alongside a summary of the available literature on zirconolite aqueous durability. The zirconolite phase may accommodate a wide variety of tri- and tetravalent actinide and rare-earth dopants through isovalent and heterovalent solid solution, e.g.  $\text{CaZr}_{1-x}\text{Pu}_x\text{Ti}_2\text{O}_7$  or  $\text{Ca}_{1-x}\text{Pu}_x\text{ZrTi}_{2-2x}\text{Fe}_{2x}\text{O}_7$ . The progressive incorporation of actinides within the zirconolite-2M parent structure is accommodated through the formation of zirconolite polytypoids, such as zirconolite-4M or 3T, depending on the choice of substitution regime and processing route. A variety of standardised durability tests have demonstrated that the zirconolite phase exhibits exceptional chemical durability, with release rates of constituent elements typically  $<10^{-5} \text{ gm}^{-2}\cdot\text{d}^{-1}$ . Further work is required to understand the extent to which polytype formation and surrogate choice influence the dissolution behaviour of zirconolite wasteforms.

### ARTICLE HISTORY

Received 18 November 2020  
Revised 16 December 2020  
Accepted 8 January 2021



### KEYWORDS

Wasteform; zirconolite;  
ceramics; plutonium;  
immobilisation

## Introduction

The resurgence of nuclear power, as a driver towards cleaner energy production, will necessitate the implementation of advanced spent fuel management strategy, and development of advanced nuclear materials capable of safely conditioning highly radioactive waste [1–3]. After nuclear fuel is removed from a reactor, nation states have the option to chemically recover a significant portion of the fissile inventory, or treat the fuel as waste for disposal. These fuel cycle options are considered *closed* or *open* respectively; the unit operations associated with these are illustrated in Figure 1. For many years the U.K. has operated a closed fuel cycle, in which a PUREX (plutonium-uranium-reduction-extraction) reprocessing step is implemented, with the primary motive to recover U/Pu from spent fuel. In the PUREX process, nuclear fuel pins are stripped of cladding and dissolved in 9M  $\text{HNO}_3$ ; the aqueous nitric solution is then contacted with tri-butylphosphate (TBP).  $\text{U}^{6+}$  and  $\text{Pu}^{4+}$  form TBP complexes and are extracted to the organic phase;  $\text{U}^{6+}$  and  $\text{Pu}^{4+}$  are converted to oxides and calcined before storage. The remaining aqueous nitrate solution is comprised predominantly of high fission products and metalloids (Cs, I, Sr, As, Nd, Pd, Pr, Eu, La, Gd), minor actinides (Cm, Am, Np, Th),

corrosion products (Mn, Ni, Cr), and entrained U/Pu. This effluent is referred to as high level liquid waste (HLLW) and is stored on the Sellafield site, before blending and calcination, prior thermal conditioning. The HLLW remains highly radioactive due to the long halflife of certain elements (e.g.  $t_{1/2}^{237}\text{Np} = 2.1 \times 10^6 \text{ y}$ ,  $t_{1/2}^{129}\text{I} = 1.57 \times 10^7 \text{ y}$ ). The current baseline thermal treatment for HLLW is vitrification in alkali borosilicate glass. In the vitrification process, HLLW is calcined and melted with glass forming additives, allowing complete dissolution of waste species into the vitrified network via incorporation into the glass forming structure; incorporation as network modifiers; and incorporation by encapsulation [4]. Although borosilicate glasses can incorporate a wide variety of elements, and vitrification is a well-established process that remains relatively insensitive to variations in feedstock chemistry, it is not the optimal choice for waste streams consisting of high actinide fractions, such as waste  $\text{PuO}_2$ . Actinides have exhibited low solubility in borosilicate glass matrices, alongside leach rates that are considerably higher than alternate wasteforms such as crystalline ceramics. The  $\text{Pu}^{4+}$  solubility in the French R7T7 glass has been limited at around 1.5 wt-% [5]. Several notable publications have indicated the solubility of plutonium can be increased to 4 wt-% when reduced to the Pu(III)

**CONTACT** Lewis R. Blackburn  [lewis.blackburn@sheffield.ac.uk](mailto:lewis.blackburn@sheffield.ac.uk)  Immobilisation Science Laboratory, Department of Materials Science and Engineering, University of Sheffield, Sir Robert Hadfield Building, Mappin Street, S1 3JD, UK; Neil C. Hyatt  [n.c.hyatt@sheffield.ac.uk](mailto:n.c.hyatt@sheffield.ac.uk)  Immobilisation Science Laboratory, Department of Materials Science and Engineering, University of Sheffield, Sir Robert Hadfield Building, Mappin Street, S1 3JD, UK

© 2021 The Author(s). Published by Informa UK Limited, trading as Taylor & Francis Group

This is an Open Access article distributed under the terms of the Creative Commons Attribution-NonCommercial-NoDerivatives License (<http://creativecommons.org/licenses/by-nc-nd/4.0/>), which permits non-commercial re-use, distribution, and reproduction in any medium, provided the original work is properly cited, and is not altered, transformed, or built upon in any way.

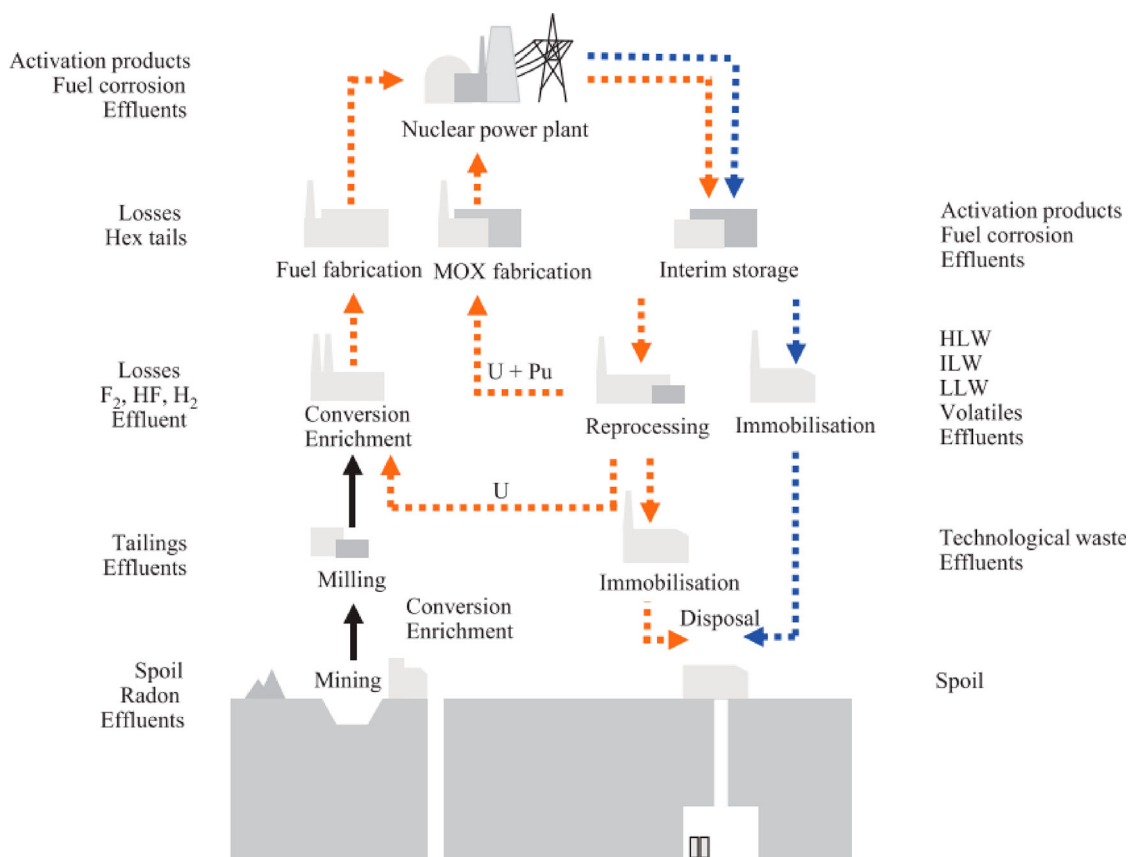


**Figure 1.** Illustration of unit operations associated with open and closed nuclear fuel cycles. Orange arrows indicate closed fuel cycle operations, while blue arrows represent those for an open fuel cycle (© IOP Publishing. Reproduced with permission. All rights reserved. [10]).

species [5–7]. A series of borosilicate glasses containing 1 wt-%  $PuO_2$  were fabricated Wellman et al. in order to elucidate the effect of self-irradiation on the elemental dissolution of the glass phase. Although it was determined that the release rate of Pu into the extraction phase was insensitive to dose rate (measured by  $^{238}Pu/^{239}Pu$  ratio), temperature, and pH, was of the order  $10^{-3} gm^{-2}d^{-1}$  [8]. The development of SYNROC technology (synthetic-rock) in the 1980s has led to development of alternative wasteforms for nuclear

waste based on ceramic systems [9]. The SYNROC formulation comprises an assemblage of chemically durable titanate crystalline phases (zirconolite, hollandite, perovskite, pyrochlore), based on natural mineral hosts that have demonstrated resistance to weathering on geological timescales; these can act as dedicated hosts for specific elements via accommodation in specific lattice sites in the host phase, providing a marked increase in solubility and chemical durability. The host phase for actinides is zirconolite – nominally  $CaZrTi_2O_7$ . The aim of this work is to provide an extensive literature review into the suitability of the zirconolite phase as a host for  $PuO_2$ . An assessment of the current UK situation regarding Pu will first be outlined, followed by a critical assessment of zirconolite as a ceramic host phase for Pu.

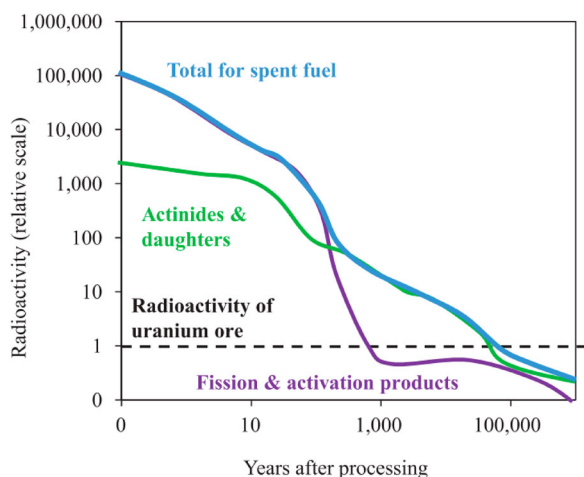


**Figure 2.** Illustration of timescales necessary for geological disposal (© IOP Publishing. Reproduced with permission. All rights reserved [10]).

### Actinide immobilisation in ceramic materials

Owing to their relatively long half-lives and radiotoxicity, radionuclides must be separated from the biosphere and permanently disposed. The current intended disposal route for many countries is deep geological disposal, in an engineered repository known as a geological disposal facility (GDF). A GDF utilises the multibarrier concept, wherein a series of engineered barriers are constructed to prevent the

**Table 1.** Mineral host phases for actinide species.

Mineral	Ideal composition	Mineral space group	Calculated density (g/cm <sup>3</sup> )	References
Pyrochlore	A <sub>2</sub> B <sub>2</sub> O <sub>7</sub> (e.g. Gd <sub>2</sub> Ti <sub>2</sub> O <sub>7</sub> )	Fd-3m	6.57	[27–36]
Zircon	ZrSiO <sub>4</sub>	I4 <sub>1</sub> /amd	4.66	[37–42]
Zirconia	ZrO <sub>2</sub>	P2 <sub>1</sub> /c	5.82	[43–49]
Zirconolite	CaZrTi <sub>2</sub> O <sub>7</sub>	C2/c	4.44	[33,50–64]
Monazite	CePO <sub>4</sub>	P2 <sub>1</sub> /n	5.26	[65–74]
Perovskite	CaTiO <sub>3</sub>	Pbnm	4.04	[75–81]
Brannerite	UTi <sub>2</sub> O <sub>6</sub>	C2/m	6.37	[82–90]

egress of radionuclides until the radioactive output of the waste has decayed to levels comparable to the original uranium ore from which uranium fuel is derived, see Figure 2. The primary containment for radionuclides in this scenario is known as the *wasteform*, a passively safe material designed to prevent the release of radionuclides. Proposed wasteforms include cementitious, glass, ceramic, and glass-ceramic composite materials. Comprehensive analyses of these materials for nuclear waste applications are provided elsewhere [4,11–20]. In the context of the immobilisation of actinides, e.g. Pu, ceramic materials are considered to offer performance, including waste-loading and aqueous durability, when compared to cement-based systems, typically used for encapsulation of intermediate level wastes (ILW) and borosilicate glasses used for high level waste (HLW) immobilisation [12,16,19,21,22]. There have been many notable publications investigating potential single phase and multiphase ceramic wasteforms for the immobilisation of actinides, a selection of proposed host matrices for actinides is given in Table 1. Titanate and zirconate minerals have been particularly well-studied as a result of their excellent resistance to chemical alteration, and relatively high degree of resistance to radiation induced amorphisation [23–26]. Actinide incorporation in ceramic phases is achieved by allowing the waste component to be readily accepted into solid solution in the host lattice, either by direct substitution or partial incorporation with an appropriate charge compensation mechanism. Generally, the choice of solid solution mechanism is dictated by the relative ionic radii of the radionuclide and host cation site, and accessible valence states. For example, the zirconolite structure may accept Pu<sup>4+</sup> in solid solution via homovalent substitution for Zr<sup>4+</sup>, i.e. CaZr<sub>1-x</sub>Pu<sub>x</sub>Ti<sub>2</sub>O<sub>7</sub>, or by a coupled substitution if Pu<sup>4+</sup> is substituted for Ca<sup>2+</sup>, with a secondary lower valence cation included to maintain charge balance, i.e. Ca<sub>1-x</sub>Pu<sub>x</sub>ZrTi<sub>2-x</sub>Mg<sub>x</sub>O<sub>7</sub>.

The design and implementation of ceramic actinide wasteforms is contingent on the following criteria:

- **Wasteloading:** The ceramic composition should be tailored such that solubility of waste material in the host phase is as extensive as reasonably possible,

without the formation of deleterious secondary phases. This will alleviate space requirements in a geological disposal facility, through the reduction in the number of overall waste packages produced. The ceramic should also be able to incorporate appropriate quantity of Gd<sup>3+</sup> and/or Hf<sup>4+</sup>, to act as a neutron poison in the final Pu-bearing wasteform.

- **Fabricability:** Advantage should be taken of established manufacturing techniques, placing emphasis on the utilisation of continuous and simple processes. The use of exotic processing routes and high temperature thermal treatments should be avoided, if feasible.
- **Criticality:** The prevention of post immobilisation criticality must be ensured by the addition of a suitable quantity of neutron poison (e.g. Hf, Gd). The wasteform must be able to accommodate the co-incorporation of these species, and without significantly altering the waste package integrity or the host phase assemblage. There is currently no defined standard in the UK for the concentration of neutron poisons present in ceramic wasteforms for Pu immobilisation.
- **Proliferation Resistance:** The resulting waste package must demonstrate suitable resistance against illicit recovery of fissile material. This could potentially be achieved by a combination of the use of a multi-barrier overpack, and the production of a ceramic from which Pu extraction would be difficult and undesirable.
- **Aqueous Durability:** The chemical durability of the host material is essential in understanding the dissolution and long-term release rates of radionuclides to the wider environment. Wasteforms should be designed such that corrosion via groundwater ingress to the waste package occurs in manner that is minimised, controlled and predictable. Considering the half-life of <sup>239</sup>Pu is approximately 24,100 years, a containment period of at least 10 half-lives would be required, thus 241,000 years. The wasteform must therefore demonstrate high resistance to leaching under repository conditions for timescales of this magnitude.
- **Radiation Tolerance:** Ceramic wasteforms should demonstrate suitable resistance to the effects of irradiation induced by radioactive decay of waste components contained within the host structure.

## Zirconolite ceramics for Pu immobilisation

### Crystal structure of zirconolite

Zirconolite, ideal composition CaZrTi<sub>2</sub>O<sub>7</sub> ( $\rho = 4.44 \text{ g}\cdot\text{cm}^{-3}$ ,  $Z = 8$ , space group C2/c) is a relatively rare accessory mineral that has been located in a variety of terrestrial geologies, with a demonstrated affinity for, but not limited to, U<sup>4+</sup>, Th<sup>4+</sup>, Ce<sup>3+/4+</sup>, Al<sup>3+</sup>, Pu<sup>3+/4+</sup>, Gd<sup>3+</sup> and Hf<sup>4+</sup>. Confidence in the zirconolite

wasteform to successfully act as a host for actinides is largely underpinned through the existence of nature specimens, which have demonstrated excellent resistance to natural weathering effects over geological timescales, with several specimens found to retain significant portions of their primordial actinide inventories ( $\sim 20$  wt-% U/Th) [33, 91–94]. The ideal zirconolite structure is an anion-deficient fluorite superstructure, and is considered to be a derivative of the pyrochlore family of minerals, with approximate formulation  $(\text{Ca}, \text{Na}, \text{Ce}, \text{Th})_2(\text{Nb}, \text{Ta}, \text{Ti})_2\text{O}_6(\text{OH}, \text{F})$ , however this often generalised to  $\text{A}_2\text{B}_2\text{O}_7$  ( $Z = 8$ , space group  $\text{Fd-}3\text{m}$ ) where A is typically some trivalent  $\text{REE}^{3+}$  species and  $\text{B}^{4+} = \text{Ti}, \text{Zr}$  [30,95,96]. During the development of the SYNROC wasteform, zirconolite was included as the host phase for actinides, due to its high aqueous durability [26,97–100]. Accordingly, a significant body of work has since been undertaken in order to determine the solubility of a wide array of actinide and rare-earth cation species within the zirconolite framework, particularly Ce and U as surrogates for Pu. The ideal zirconolite unit cell is comprised of planes of corner sharing  $\text{CaO}_8$  and  $\text{ZrO}_7$  polyhedra, interleaved by hexagonal tungsten bronze (HTB) type layers along (001).  $\text{Ti}^{4+}$  is distributed across three distinct sites in the HTB plane, two of which are  $\text{TiO}_6$  octahedra, and one of which is a 50% statistically occupied  $\text{TiO}_5$ , giving rise to trigonal bipyramidal coordination [101]. In this idealised structural description (see Figure 3), cation and HTB layers are integrated 1:1 along (001), related by a  $180^\circ$  rotation along the  $c^*$  axis. Owing to this two-layer repeat, stoichiometric  $\text{CaZrTi}_2\text{O}_7$  is commonly referred to as zirconolite-2M, with reference to the two layer lamellar monoclinic motifs comprising the unit cell. The zirconolite-2M polytype has been since been demonstrated to form over the compositional range  $\text{CaZr}_x\text{Ti}_{3-x}\text{O}_7$  for  $0.83 \leq x \leq 1.33$ , indicating considerable flexibility with regards to  $[\text{Ti}]/[\text{Zr}]$  ratio [102]. The distribution of Ti across cation sites in zirconolite has also been shown to be controlled as a

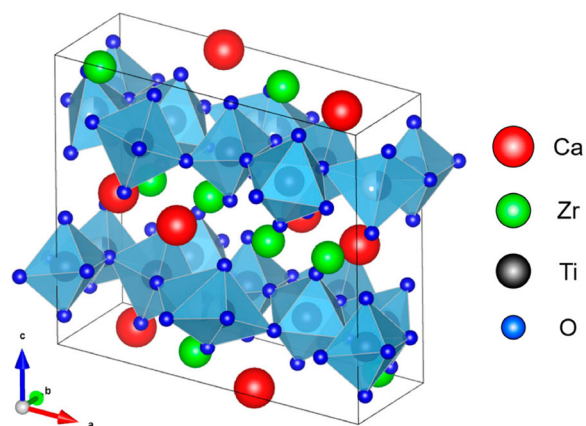


**Figure 3.** Crystal structure of zirconolite-2M ( $\text{CaZrTi}_2\text{O}_7$ ).

function of sample preparation temperature [52]. Zirconolite also exhibits a number of crystallographically distinct polytype structures, the formation of which is observed to be controlled by the chosen substitution regime and oxygen fugacity during synthesis. Zirconolite polytyoids are characterised by variation in stacking sequence of adjacent Ca/Zr and HTB layers, for example, the zirconolite-4M structure was solved by Coelho et al. as a four layer repeating sequence, comprised of alternating zirconolite-2M and pyrochlore-type layers, resulting in a doubling of the unit cell along the  $c$ -axis, retaining monoclinic symmetry [103]. Extensive substitution of Pu within the  $\text{Ca}^{2+}$  site, facilitated by co-substitution of  $\text{Fe}^{3+}$  was reported by Gilbert et al. to produce the trigonal zirconolite-3T variation (space group  $\text{P}3_121$ ) [104]. Polytypes adopting three and six-layer orthorhombic symmetry have also been reported, but detailed structural solutions are lacking [64].  $\text{Ca}^{2+}$  and  $\text{Zr}^{4+}$  sites are of particular interest as both have been shown to readily accept a range of actinide and rare-earth elements [53,55,56,64,78,105–108]. Extensive solubility of  $\text{Mg}^{2+}$ ,  $\text{Al}^{3+}$ ,  $\text{Ti}^{3+}$ ,  $\text{Fe}^{3+}$ , and  $\text{Nb}^{5+}$  species within the  $\text{Ti}^{4+}$  site has also been demonstrated, with the view to charge balance substitutions which do not exhibit iso- valence across the structure, e.g. the accommodation of Pu within the  $\text{Ca}^{2+}$  site could be achieved by the co-substitution of  $\text{Al}^{3+}$  via  $\text{Ca}_{1-x}\text{Pu}_x\text{ZrTi}_{2-2x}\text{Al}_{2x}\text{O}_7$ , assuming all Pu is present as  $\text{Pu}^{4+}$  [55,98,104,109]. The simultaneous substitution of trivalent species within both  $\text{Ca}^{2+}$  and  $\text{Zr}^{4+}$ , negating the need for charge balancing species, has also been demonstrated [110–113]. As the manipulation of Pu in wasteform development trials is not often possible, due to the stringent handling requirements associated with radiotoxicity and the handling of fissile material, the remainder of this review will aim to provide a comprehensive discussion of Ce and U surrogate incorporation in zirconolite.

### **Incorporation of Ce in zirconolite**

#### **Incorporation of Ce within $\text{Zr}^{4+}$ site**

The formation of zirconolite with Ce targeted in the  $\text{Zr}^{4+}$  site ( $\text{CaZr}_{0.8}\text{Ce}_{0.2}\text{Ti}_2\text{O}_7$ ) was attempted by Begg and Vance [114]. Two distinct zirconolite phases were observed to form (zirconolite-2M and zirconolite-4M) alongside a secondary perovskite phase with considerable incorporated Ce (calculated stoichiometry  $\text{Ca}_{0.72}\text{Ce}_{0.24}\text{Zr}_{0.02}\text{Ti}_{1.03}\text{O}_3$ ). Ce  $\text{L}_{\text{III}}$  edge X-ray absorption spectra (XANES) confirmed the presence of 35%  $\text{Ce}^{3+}$ , despite extended sintering under oxidising conditions. Further annealing in air at lower temperatures resulted in total conversion to  $\text{Ce}^{4+}$ , inferring the excess positive charge in the zirconolite-2M species may be self-compensated by cation vacancies. This work was complemented by Blackburn et al.

with the  $\text{CaZr}_{1-x}\text{Ce}_x\text{Ti}_2\text{O}_7$  system synthesised under both oxidising and reducing conditions [115]. It was determined that sintering at 1350°C under oxidising conditions produced a transformation to zirconolite-4M above  $x = 0.20$ , although failed to stabilise the entire Ce inventory as  $\text{Ce}^{4+}$ , with 28% Ce manifested as  $\text{Ce}^{3+}$ . Synthesising the solid solution under a 5%  $\text{H}_2/\text{N}_2$  mixture promoted the formation of a Ce-rich perovskite phase, bypassing the formation of zirconolite-4M at the result of uniform  $\text{Ce}^{3+}$  speciation. Blackburn et al. also fabricated a sample corresponding to nominal composition  $\text{CaZr}_{0.80}\text{Ce}_{0.20}\text{Ti}_2\text{O}_7$  by hot isostatic pressing (1300°C dwell temperature, maintained for 4 h with isostatic pressure 100 MPa) [116]. The bulk matrix was of near theoretical density, with zirconolite-2M comprising  $\sim 81$  wt-% of the phase assemblage, with the remainder comprised of zirconolite-4M and Ce-perovskite. Similar phase fields were reported in the  $\text{CaZr}_{1-x}\text{Ce}_x\text{Ti}_2\text{O}_7$  system by Clark et al. utilising both conventional sintering and spark plasma sintering (SPS) [56]. Accommodation of Ce ( $x \geq 0.20$ ) resulted in the formation of zirconolite-4M. EDS measurements confirmed that greater Ce content was concentrated in the zirconolite-4M phase, with a secondary Ce-bearing perovskite phase produced due to partial  $\text{Ce}^{3+}$  speciation. At extensive targeted Ce-substitution ( $x = 0.5$ ), zirconolite-4M was present at high concentration (96 wt-%). The reducing conditions imposed by the SPS process promoted  $\text{Ce}^{4+}$  reduction to  $\text{Ce}^{3+}$ , destabilising zirconolite-4M in favour of Ce-rich perovskite. The  $\text{CaZr}_{1-x}\text{Ce}_x\text{Ti}_2\text{O}_7$  solid solution was extended by Li et al. [51]. A structural transformation from the zirconolite-2M to the zirconolite-4M polytype was observed, alongside accessory perovskite, in line with previous observations. Further attempted incorporation of Ce within the Zr site yielded a cubic pyrochlore phase (ideal composition  $\text{CaCeTi}_2\text{O}_7$ ), and the total solubility limit of Ce was determined to be approximately  $x = 0.80$ . X-ray photoelectron spectroscopy (XPS) analysis confirmed the ratio of  $\text{Ce}^{3+}/\text{Ce}^{4+}$  to decrease from 1.24 at low concentration ( $x = 0.20$ ) to 0.45 at maximum Ce concentration ( $x = 1.00$ ).

### **Incorporation of Ce in $\text{Ca}^{2+}$ site with charge compensators**

Ce substitutions into zirconolite were undertaken by Begg and Vance, with the successful synthesis of  $\text{Ca}_{0.8}\text{Ce}_{0.2}\text{ZrTi}_{1.6}\text{Al}_{0.4}\text{O}_7$  by sintering in air at 1400°C [114]. XANES measurements confirmed that  $\text{Ce}^{4+}$  was present at only 70%. Minor  $\text{Al}_2\text{O}_3$  was also formed, hence  $\text{Al}^{3+}$  charge compensation was only therefore sufficient for 70%  $\text{Ce}^{4+}$ . Furthermore, re-formulation targeting  $\text{Ce}^{3+}$  on the  $\text{Ca}^{2+}$  site, producing a stoichiometry of  $\text{Ca}_{0.8}\text{Ce}_{0.2}\text{ZrTi}_{1.8}\text{Al}_{0.2}\text{O}_7$  formed a single phase zirconolite, in which  $\text{Ce}^{3+}$  was accommodated entirely on the  $\text{Ca}^{2+}$  site. Further work by Begg et al.

determined that zirconolite could undergo self-charge compensation via the formation of cation vacancies and trivalent  $\text{Ti}^{3+}$ , under oxidising and reducing conditions respectively [80]. This was demonstrated by the synthesis of single phase  $\text{Ca}_{0.9}\text{Ce}_{0.1}\text{ZrTi}_2\text{O}_7$  under both oxidising and reducing conditions (i.e. the incorporation of  $\text{Ce}^{3+}$  and  $\text{Ce}^{4+}$  on the  $\text{Ca}^{2+}$  site), displaying an apparent excess charge. Vance et al. confirmed that  $\text{Ce}^{3+}$  may be overwhelmingly incorporated into the  $\text{Ca}^{2+}$  site, when reacting under reducing conditions, forming a single phase up to 0.3 f.u., i.e.  $\text{Ca}_{0.70}\text{Ce}_{0.30}\text{ZrTi}_{1.70}\text{Al}_{0.30}\text{O}_7$  [117]. Similar results were obtained by Kaur et al. targeting  $\text{Ca}_{0.80}\text{Ce}_{0.20}\text{ZrTi}_{1.80}\text{Al}_{0.20}\text{O}_7$ , with synthesis under air at 1400°C. Ce was observed to fully accommodate within the zirconolite-2M phase, with XPS analysis confirming the formation of 75%  $\text{Ce}^{3+}$ , with sufficient  $\text{Al}^{3+}$  to charge balance [118]. Similar processing techniques were utilised by Pöml et al. targeting  $\text{Ce}^{4+}$  and  $\text{Al}^{3+}$  accommodation; specimens were sintered at 1400°C for 2 d [119]. Near single phase specimens with nominal composition  $\text{Ca}_{0.85}\text{Ce}_{0.15}\text{ZrTi}_{1.70}\text{Al}_{0.30}\text{O}_7$  and  $\text{Ca}_{0.87}\text{Ce}_{0.13}\text{ZrTi}_{1.74}\text{Al}_{0.36}\text{O}_7$  were fabricated by solid state synthesis, with EELS data confirming the formation of 80%  $\text{Ce}^{3+}$ , without a change in phase assemblage. A complementary investigation of the efficacy of  $\text{Cr}^{3+}$  as a charge balancing species was reported by Blackburn et al., with the  $\text{Ca}_{1-x}\text{Ce}_x\text{ZrTi}_{2-2x}\text{Cr}_{2x}\text{O}_7$  solid solution synthesised in air at 1350°C [120]. Single phase specimens were produced in the interval  $0.05 \leq x \leq 0.20$ , after which  $\text{Cr}_2\text{O}_3$ ,  $\text{CeO}_2$  and a Ce-rich perovskite phase were observed in the microstructure, although when targeting  $x = 0.35$  the zirconolite-2M phase remained present at  $\sim 94$  wt-%. Selected area electron diffraction confirmed that the 2M polytype structure was maintained throughout the phase evolution. Ce  $L_3$  XANES data confirmed partial reduction to  $\text{Ce}^{3+}$  varying between 15% and 27%, similar to previous studies.

### **Incorporation of U/Pu in zirconolite**

#### **Incorporation of U/Pu in $\text{Zr}^{4+}$ site**

During development of SYNROC technology, U and Pu were observed to partition overwhelmingly into the zirconolite phase, although explicit discussion of zirconolite polytype formations were not provided [99,121,122]. Although more recent attempts to fabricate titanate phase assemblages by hot isostatic pressing, targeting a high zirconolite fraction, report agreeable data [123,124], it is necessary to discuss the structural effects of U/Pu incorporation within the zirconolite phase in isolation. Kesson et al. reported the solid solution limits of U within the zirconolite structure, targeting substitution on the  $\text{Zr}^{4+}$  site [98]. Compositions corresponding to  $\text{CaZr}_{0.75}\text{U}_{0.25}\text{Ti}_2\text{O}_7$ ,  $\text{CaZr}_{0.50}\text{U}_{0.50}\text{Ti}_2\text{O}_7$  were fabricated by

hot pressing at 1400°C; zirconolite and pyrochlore were yielded in each instance. Attempting to partition a greater amount of U within the  $Zr^{4+}$  site promoted the formation of the pyrochlore phase, alongside secondary (Ti,Zr,U)O<sub>2</sub> solid solutions. Initial work by Vance et al. reported the incorporation of 0.5 f.u. of U within the  $Zr^{4+}$  site, targeting CaZr<sub>0.5</sub>U<sub>0.5</sub>Ti<sub>2</sub>O<sub>7</sub>, by hot pressing at 1250°C, followed by a 1400°C heat treatment under reducing conditions, with a view to stabilise U<sup>4+</sup> [106]. Further substitution of U appeared to stabilise the pyrochlore structure, while a minor U-containing rutile was also formed in all concentrations. The crystal chemistry of the uranium pyrochlore (CaU<sup>4+</sup>Ti<sub>2</sub>O<sub>7</sub> – betafite) is discussed elsewhere [125]. The CaZr<sub>0.80</sub>U<sub>0.20</sub>Ti<sub>2</sub>O<sub>7</sub> composition was also produced by HIP (1300°C, 100 MPa) by Blackburn et al. yielding a significant fraction of zirconolite-2M (~ 97 wt-%), alongside minor unincorporated UO<sub>2</sub> and a (Zr,U)O<sub>2</sub> solid solution [116]. A detailed investigation of U<sup>4+</sup> accommodation in the zirconolite CaZr<sub>1-x</sub>U<sub>x</sub>Ti<sub>2</sub>O<sub>7</sub> system was performed by Vance et al. in 2002 [55]. Synthesis of the solid solution under inert conditions produced single phase zirconolite-2M when targeting  $x = 0.10$ , with the zirconolite-4M phase preferred above  $x = 0.20$ . Further U<sup>4+</sup> concentration increased the relative yield of the zirconolite-4M phase, with extensive incorporation (~0.5 f.u. U<sup>4+</sup>) producing the U-pyrochlore phase, in line with previous data. Oxidation of samples corresponding to CaZr<sub>0.9</sub>U<sub>0.1</sub>Ti<sub>2</sub>O<sub>7</sub> and CaZr<sub>0.8</sub>U<sub>0.2</sub>Ti<sub>2</sub>O<sub>7</sub> promoted the formation of U<sup>5+</sup>, causing the destabilisation of the zirconolite-4M phase with respect to the zirconolite-2M structure. Shrivastava, Kumar and Sharma have provided an excellent structural refinement of the zirconolite-2M CaZr<sub>0.95</sub>U<sub>0.05</sub>Ti<sub>2</sub>O<sub>7</sub> and CaZr<sub>0.90</sub>U<sub>0.10</sub>Ti<sub>2</sub>O<sub>7</sub> compositions [126]. More recently, the CaZr<sub>1-x</sub>U<sub>x</sub>Ti<sub>2</sub>O<sub>7+x</sub> solid solution was prepared by Subramani et al., with all compositions prepared in air at 1400°C [127]. Interestingly, zirconolite-2M was observed to form as a single phase at each level of targeted U concentration, with the average oxidation state of U close to U<sup>6+</sup> in all instances, as determined by U L<sub>3</sub> XANES. The incorporation of Pu<sup>4+</sup> within the  $Zr^{4+}$  site appears to yield broadly similar results to the corresponding U solid solution, demonstrating the efficacy of U<sup>4+</sup> as a structural surrogate under inert conditions. Structural effects of Pu<sup>4+</sup> substitution within the  $Zr^{4+}$  site in zirconolite were investigated by Begg et al. [105]. When sintering in air, CaZr<sub>0.9</sub>Pu<sub>0.1</sub>Ti<sub>2</sub>O<sub>7</sub> was successfully synthesised as a single phase, with a secondary Pu-rich zirconolite-4M phase formed above  $x = 0.20$ . The yield of zirconolite-4M was increased with further Pu<sup>4+</sup> substitution; a pyrochlore phase was observed to crystallise for the phase corresponding to CaZr<sub>0.60</sub>Pu<sub>0.40</sub>Ti<sub>2</sub>O<sub>7</sub>. Annealing specimens under reducing conditions (3.5% H<sub>2</sub>/N<sub>2</sub> – 1200°C) promoted the

formation of Pu<sup>3+</sup>, similar to Ce, however this reduction mechanism is not available for U, highlighting a caveat for the deployment of U as a Pu surrogate under reducing conditions. The accompanying increase in ionic radius was considered to cause the destabilisation of the zirconolite-4M phase, with respect to zirconolite-2M, stabilising a deleterious perovskite phase in agreement with cerium doped specimens, in which targeting  $Zr^{4+}$  substitution for Ce<sup>3+</sup> promoted the formation of perovskite. Complementary results were obtained by Vance et al. targeting CaZr<sub>0.50</sub>Pu<sub>0.50</sub>Ti<sub>2</sub>O<sub>7</sub>; hot pressing the sample (i.e. reducing conditions) yielded approximately 50 wt-% Pu-perovskite attributed to the formation of Pu<sup>3+</sup> [106]. Further work by Begg et al. confirmed that hot pressing the CaZr<sub>0.80</sub>Pu<sub>0.20</sub>Ti<sub>2</sub>O<sub>7</sub> composition failed to produce a single phase product, with only 50 wt-% zirconolite yield attributed to uniform Pu<sup>3+</sup> speciation [26,128]. Nevertheless, annealing the composition in air at 1300°C produced significant modifications to the phase assemblage, yielding ~ 80 wt-% zirconolite, alongside a Pu-rich pyrochlore phase, eliminating the perovskite phase.

#### ***Incorporation of U/Pu in Ca<sup>2+</sup> site with charge compensators***

A selection of zirconolites targeting U<sup>4+</sup> incorporation within the Ca<sub>1-x</sub>U<sub>x</sub>ZrTi<sub>2-2x</sub>Al<sub>2x</sub>O<sub>7</sub> system were synthesised by Vance et al. with a view to further extend U<sup>4+</sup> solubility without structural transformation to the closely related pyrochlore phase [117]. The solubility limit was determined to be  $0.3 \leq x \leq 0.4$ , after which further accommodation of U<sup>4+</sup> resulted in the formation of UO<sub>2</sub>-ZrO<sub>2</sub> solid solutions, and minor Al<sub>2</sub>O<sub>3</sub>. Further work demonstrated that imposing reducing conditions by hot pressing yielded a secondary brannerite phase, at appreciable quantity [106]. A more systematic approach was later undertaken, in which both Al<sup>3+</sup> and Mg<sup>2+</sup> were targeted on the Ti<sup>4+</sup> site in order to provide sufficient charge compensation for both U<sup>4+</sup> and U<sup>5+</sup> [55]. It was determined that single phase zirconolite-2M was formed in both instances when targeting values  $x = 0.1, 0.2$ , after which secondary formation of UTi<sub>2</sub>O<sub>6</sub>, ZrO<sub>2</sub> and UO<sub>2</sub> phases was observed. The use of Mg<sup>2+</sup> to charge balance approximately 26 wt-% U<sup>4+</sup> in the zirconolite structure was reported by Kesson et al. with U apparently distributed between Ca<sup>2+</sup> and  $Zr^{4+}$  sites [98]. The targeted zirconolite stoichiometry was not reported. Pu-bearing zirconolites targeting Ca<sup>2+</sup> substitution without charge compensation (i.e. Ca<sub>0.9</sub>Pu<sub>0.1</sub>HfTi<sub>2</sub>O<sub>7</sub> –  $Zr^{4+}$  entirely replaced by Hf<sup>4+</sup>) were prepared by Begg, Vance and Conradson [78]. Pu was accommodated across both Ca<sup>2+</sup> and Hf<sup>4+</sup> sites, contrary to design; annealing under reducing conditions did not stabilise the formation of a secondary perovskite phase, despite 80% reduction to Pu<sup>3+</sup>. Deschanel's



et al. confirmed the synthesis of single phase  $\text{Ca}_{0.87}\text{Pu}_{0.13}\text{ZrTi}_{1.73}\text{Al}_{0.30}\text{O}_7$ , exhibiting the zirconolite-2M structure, when targeting  $\text{Pu}^{4+}$  [53]. A similar composition was synthesised by Vance et al.:  $\text{Ca}_{0.80}\text{Pu}_{0.20}\text{ZrTi}_{1.80}\text{Al}_{0.20}\text{O}_7$ , configured to accommodate  $\text{Pu}^{3+}$  [106]. While conventional sintering yielded a single phase zirconolite specimen, hot pressing at  $1250^\circ\text{C}$  yielded a secondary perovskite phase. Begg et al. determined the influence of processing atmosphere in the formulation of  $\text{Pu}^{3+}$  and  $\text{Pu}^{4+}$  doped zirconolites targeting  $\text{Ca}_{0.80}\text{Pu}_{0.20}\text{HfTi}_{1.80}\text{Al}_{0.20}\text{O}_7$  and  $\text{Ca}_{0.80}\text{Pu}_{0.20}\text{HfTi}_{1.60}\text{Al}_{0.40}\text{O}_7$ , respectively, with Hf in place of Zr [128]. Targeting  $\text{Ca}_{0.80}\text{Pu}_{0.20}\text{HfTi}_{1.80}\text{Al}_{0.20}\text{O}_7$  while sintering under a 3.5%  $\text{H}_2/\text{N}_2$  mixture promoted uniform  $\text{Pu}^{3+}$  speciation, yielding approximately 88% zirconolite, alongside a Pu-perovskite phase. Sintering under air was sufficient to allow uniform  $\text{Pu}^{4+}$  valence, with  $\sim 96\%$  zirconolite yield. Synthesis of the  $\text{Ca}_{0.80}\text{Pu}_{0.20}\text{HfTi}_{1.60}\text{Al}_{0.40}\text{O}_7$  composition, requiring  $\text{Pu}^{4+}$ , failed to yield above 77% zirconolite when sintered under reducing conditions, whereas 94% zirconolite yield was produced in air.  $\text{Fe}^{3+}$  was deployed as a charge compensator in Pu-doped zirconolite, investigated by Gilbert et al. targeting  $\text{Ca}_{1-x}\text{Pu}_x\text{ZrTi}_{2-2x}\text{Fe}_{2x}\text{O}_7$  [104]. A transformation from zirconolite-2M to zirconolite-3T was reported for compositions above  $x=0.20$ , with separated  $\text{PuO}_2$  identified above  $x=0.40$ .

### Chemical durability of zirconolite

In the geological disposal scenario, aqueous dissolution of the immobilisation matrix, through contact with groundwater, will be the dominant mechanism by which radionuclides are released into the near field environment. Therefore, the design philosophy of nuclear wastefoms stipulates that chemical durability should be a primary factor when considering immobilisation matrices for actinides. Assessing the relative durability of potential wastefoms on time-scales comparable to those likely to be imposed in geological timescales presents a significant technical challenge in a laboratory setting, as these tests typically occur on the timescale of several weeks to months. A further challenge is posed by the refractory nature of many oxide ceramics, for which the durability may be several orders of magnitude greater than vitrified or cementitious matrices, depending on the material of choice [129]. Nevertheless, information regarding the long-term behaviour may be extrapolated through the use of accelerated leaching techniques, in which the wastefom is contacted with low pH solution and increased saturation temperatures. A summary of established wastefom durability tests commonly applied to ceramic and vitrified materials is listed in Table 2. Normalised leach rates of constituent elements are typically quoted in  $\text{gm}^{-2}\cdot\text{d}^{-1}$ .

**Table 2.** Examples of dissolution methodologies used to ascertain the durability of candidate nuclear wastefoms.

Durability test	Summary of conditions
MCC-1	Saturation of monolith in ASTM-Type I $\text{H}_2\text{O}$ (S.A./V = $10\text{ m}^{-1}$ ) at 40, 70 or $90^\circ\text{C}$ for 7 d.
MCC-2	As with MCC-1, yet environmental temperature may be raised to 110, 150 or $190^\circ\text{C}$ .
PCT-B	1 g powdered substrate ( $75\text{--}150\ \mu\text{m}$ ) in 10 mL ASTM-Type I $\text{H}_2\text{O}$ . $90^\circ\text{C}$ for 7 d.
SPFT	Dynamic solution ingress permitted by peristaltic pump, with variable flow rate, temperature and solution pH.
VHT	Monolith suspended in saturated water vapour to promote accelerated surface alteration.

As zirconolite comprised a significant portion of many SYNROC variations, as the primary actinide-bearing phase, a measure of zirconolite durability was obtained through evaluation of SYNROC dissolution studies. Early work by Oversby and co-workers demonstrated the comparative success of SYNROC with respect to borosilicate glasses for the immobilisation of HLW. Samples of SYNROC and PNL-76-68 waste glass (borosilicate glass with 33% simulated HLW) were studied on 0.5 g discs with distilled water at 85 and  $200^\circ\text{C}$  [130]. Release rates of 1.4 and  $8.9\ \text{gm}^{-2}\cdot\text{d}^{-1}$  were reported for the PNL-76-68 glass at 85 and  $200^\circ\text{C}$  respectively, while the upper limit for the SYNROC leach rate was determined to be several orders of magnitude lower, at  $<0.005\ \text{gm}^{-2}\cdot\text{d}^{-1}$ . Tests were repeated with powdered samples in the  $100\text{--}200\ \mu\text{m}$  size fraction to accelerate leaching; it was determined that the leach rates of U were between a factor of 5–9 lower for SYNROC at  $200^\circ\text{C}$ . In 1981, specimens of SYNROC (comprising  $\sim 35\%$  zirconolite) was crystallised by hot pressing with the addition of 20% HLW calcine readily accepted into solid solution with the constituent phases [122]. A more comprehensive investigation was performed in this instance, with variations in both temperature and leaching duration, allowing improved comparability between ceramic and glass phases for HLW immobilisation. With respect to leaching rates, SYNROC specimens were observed to decrease by approximately two orders of magnitude between 10–30 days, whereas borosilicate specimens were observed to dissolve at a consistent rate (see Figure 4). At  $95^\circ\text{C}$  the leachability of U from the SYNROC specimen was determined to be smaller than for the borosilicate glass by a factor of 100,000. A specimen of SYNROC with added 10 wt-% HLW (0.62 wt-%  $^{239}\text{Pu}$ ) was hot pressed, and subject to MCC-1 durability testing by Smith et al. with extensive leach periods of 52 d and 2472 d at  $70^\circ\text{C}$  in deionised water, alongside carbonate and silicate leachates [100]. After 52 d,  $^{239}\text{Pu}$  release rates for carbonate and silicate leachates were an order of magnitude greater than for deionised water ( $10^{-4}$ ,  $10^{-4}$ , and  $10^{-5}\ \text{gm}^{-2}\cdot\text{d}^{-1}$ , respectively). However, after 2472 d,

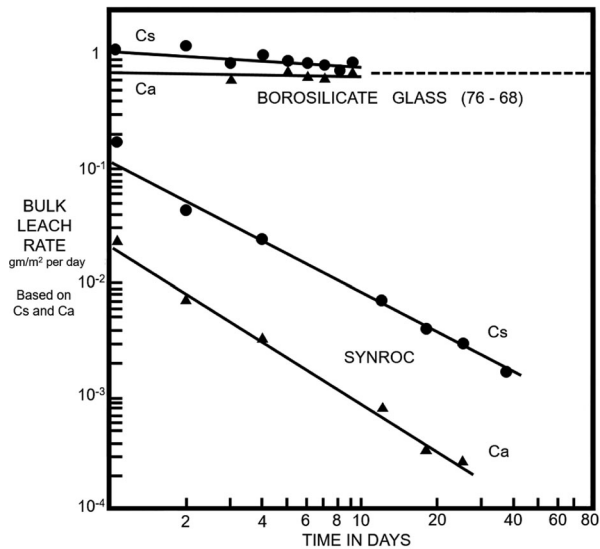


**Figure 4.** Bulk leach rate of SYNROC specimen in comparison to borosilicate glass (This article was published in A. E. Ringwood et al., "Immobilization of High-Level Nuclear Reactor Wastes in Synroc: A Current Appraisal," Nucl. Waste Manag., vol. 2, pp. 287–305, 1981, copyright Elsevier [122]).

the normalised leach rate of  $^{239}\text{Pu}$  dropped to  $10^{-6} \text{ gm}^{-2}\cdot\text{d}^{-1}$  in deionised water, demonstrating exceptional durability over extensive time periods. Further work by Smith et al. on the SYNROC wastefrom was performed using an MCC-2 dissolution assessment using deionised water, at  $150^\circ\text{C}$  [131].

Samples were loaded with 10 wt-% simulated HLW, and after 532 d, SEM analysis determined that surface layer grains of major phases exhibited no corrosion. It was confirmed that after 337 d, 0.0045% of the original Ce inventory had been released to the leachate. These early investigations were considered sufficient to demonstrate the suitability of ceramic phases for the immobilisation of nuclear wastes. However, incongruent dissolution was a key consideration, as each phase in the SYNROC assemblage did not present comparable leach rates. A variety of zirconolite-rich and pyrochlore compositions containing approximately 12 wt-% Pu (alongside 15 wt-% Hf/Gd) were synthesised by Hart et al. with release rates of Pu were measured by MCC-1 analysis at  $90^\circ\text{C}$  [23]. 7-day release rates for Pu were measured to be between  $10^{-5}$  and  $10^{-6} \text{ gm}^{-2}\cdot\text{d}^{-1}$  after 300 d, with similar release rates observed for Hf. These data provide a significant contribution towards underpinning the safety case for geological disposal of Pu in the zirconolite wastefrom, as the congruent release of Pu and neutron poisons is essential towards suppressing post-closure criticality. A zirconolite-rich titanate assemblage containing U/Th and Pu was synthesised by hot isostatic pressing by Zhang et al. yielding a zirconolite phase fraction of approximately 89 vol.-%. A secondary hollandite phase (nominally  $\text{BaAl}_2\text{Ti}_6\text{O}_{16}$ ) and  $\text{UTi}_2\text{O}_6$  brannerite phase ( $\sim 2$  vol.-%) were also formed, yet U and Th

were incorporated overwhelmingly into zirconolite, with minor uptake in the brannerite phase [123]. Pu was successfully localised within the zirconolite phase, co-substituted with Gd and Hf as neutron poisons. Both samples were subject to MCC-1 durability testing in deionised  $\text{H}_2\text{O}$  at  $90^\circ\text{C}$ , however experimental framework was modified such that the leachate was replaced after 7 and 35 days, and the test was extended to 84 days. The normalised leach rates of key elements are summarised in Figure 5. After 35 days, a normalised release rate of  $10^{-5} \text{ gm}^{-2}\cdot\text{d}^{-1}$  for Pu was measured, with similar accompanying release rates of included neutron poison species. Zirconolite-rich ceramics were synthesised by Zhang et al. by self-propagating synthesis, targeting a nominal  $\text{CaZr}_{1-x}\text{Ce}_x\text{Ti}_2\text{O}_7$  composition, with a view to assess the chemical durability of the composition corresponding to  $\text{CaZr}_{0.7}\text{Ce}_{0.3}\text{Ti}_2\text{O}_7$  by a monolithic MCC-1 test in deionised  $\text{H}_2\text{O}$  [132]. The normalised leach rate of Ce over the 42 d period was measured to be  $2.26 \times 10^{-6} \text{ gm}^{-2}\cdot\text{d}^{-1}$ , demonstrating exceptional resistance to alteration, despite the formation of a secondary Ce-bearing perovskite phase, accounting for approximately 35 wt-% of the phase assemblage. Meng et al. attempted the accommodation of Ce within both  $\text{Ca}^{2+}$  and  $\text{Zr}^{4+}$  sites, i.e.  $\text{Ca}_{1-x}\text{Zr}_{1-x}\text{Ce}_{2x}\text{Ti}_2\text{O}_7$ , anticipating the auto-reduction of Ce species may provide self-charge balance across the zirconolite structure [133]. Samples were synthesised by conventional solid state reaction and the durability was measured by PCT-B methodology. Despite a low normalised mass loss of Ce ranging between  $10^{-6}$  and  $10^{-7} \text{ gm}^{-2}\cdot\text{d}^{-1}$ , an increased order of magnitude for Ce was observed for compositions containing a greater accompanying portion of perovskite. Cerium was applied as a surrogate for Pu targeting the zirconolite phase  $\text{CaZr}_{1-x}\text{Ce}_x\text{Ti}_2\text{O}_7$  system by Wen et al. synthesised by a solid state route [134]. MCC-1 leaching

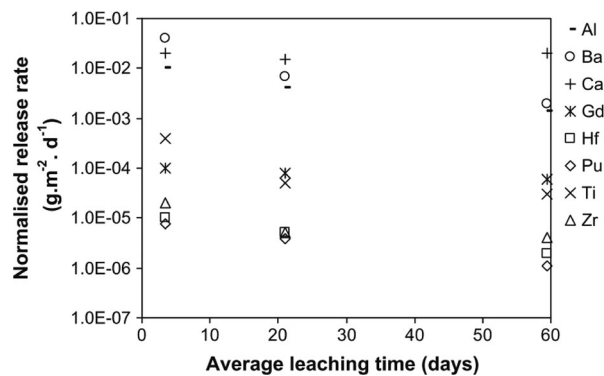


**Figure 5.** Normalised release rates of key elements for zirconolite-rich titanate assemblage processed by HIP (Reprinted from Y. Zhang et al., "Zirconolite-rich titanate ceramics for immobilisation of actinides - Waste form/HIP can interactions and chemical durability," J. Nucl. Mater., vol. 395, pp. 69–74, 2009, with permission from Elsevier [123]).

was performed on the sample pertaining to composition  $\text{Ca}_{0.76}\text{Zr}_{0.64}\text{Ce}_{0.48}\text{Ti}_{2.03}\text{O}_7$ ; the normalised leach rate for Ce was measured to be approximately  $2.3 \times 10^{-4} \text{ gm}^{-2}\cdot\text{d}^{-1}$  up to 10 days of exposure; after 28 days the leach rate decreased by two orders of magnitude to  $2.3 \times 10^{-6} \text{ gm}^{-2}\cdot\text{d}^{-1}$ . A Ce-bearing perovskite with composition  $\text{Ca}_{0.84}\text{Ce}_{0.10}\text{Ti}_{1.03}\text{O}_3$  was also stabilised, which may have attributed to a greater release fraction of Ce, hence it is unlikely that the release rates for Ce could be attributed solely to the zirconolite phase. As the formation of perovskite is a common secondary phase in the fabrication of zirconolite wasteforms, formulations must be tailored such that the accompanying fraction is minimalised. This is an issue commonly associated with cerium surrogacy, as the tendency of Ce to undergo partial reduction, despite reaction under oxidising conditions, to form  $\text{Ce}^{3+}$  is commonly observed to promote the formation of a Ce-bearing perovskite [51,56,60,114]. Perovskite (nominally  $\text{CaTiO}_3$ ) is present as a major constituent of the SYNROC assemblage, as a host for  $\text{Sr}^{2+}$ , despite markedly lower resistance to alteration with respect to the zirconolite phase. The relative leach rates of perovskite and zirconolite, with respect to pH dependence, was elucidated by McGlenn et al. subsequent to the demonstration of SYNROC for HLW immobilisation, as a precursor towards to implementation of single phase ceramic wasteforms. The formation of  $\text{TiO}_2$  (anatase) at  $90^\circ\text{C}$  on the surface of perovskite specimens was observed at low and neutral pH levels, indicating hydrothermal alteration of the perovskite phase; no evidence of dissolution was observed with XRD or SEM techniques for the zirconolite phase [135]. It has since been proposed that precipitation of  $\text{TiO}_2$  in subsequent dissolution trials was attributed to the dissociation of  $\text{CaTiO}_3$  [81,136].

Potential zirconolite formulations for Pu must incorporate sufficient buffer phases such that the formation of Pu-perovskite is not thermodynamically or kinetically favourable, as this may exacerbate the rate of Pu extraction from the wasteform in the geological disposal environment. Begg et al. synthesised perovskite incorporated with Pu under oxidising and reducing conditions, with a view to elucidate the substitution mechanism of  $\text{Pu}^{4+}$  and  $\text{Pu}^{3+}$ , respectively, within  $\text{CaTiO}_3$  [78]. Attempting to form  $\text{Ca}_{0.9}\text{Pu}_{0.1}\text{Ti}_{1.9}\text{Al}_{0.1}\text{O}_3$  under reducing conditions yielded two perovskite phases, accounting for an 80% reduction to the trivalent species. It was determined that  $\text{Pu}^{4+}$  can be substituted into the perovskite structure as a single phase in excess, with Ti vacancies allowing for charge neutrality to be preserved. Moreover, the perovskite phase was observed to accommodate a considerable amount of  $\text{Pu}^{3+}$  and  $\text{Pu}^{4+}$  without the addition of charge balancing species. Further work by Begg et al. confirmed that the release of Pu from  $\text{CaTiO}_3$  under acidic conditions was indiscriminate

of Pu valence [79]. More recently, the chemical durability of near single phase zirconolite has been elucidated. A sample of zirconolite with nominal composition  $\text{Ca}_{0.80}\text{Nd}_{0.20}\text{ZrTi}_{1.80}\text{Al}_{0.20}\text{O}_7$  was synthesised by hydrolysis of alkoxide nitrate precursor material, before calcination and sintering at  $1400^\circ\text{C}$  in air. An excess of 1.5 wt-% Ti/Zr oxides were added to discourage perovskite formation; a dense microstructure of zirconolite-2M with minor  $\text{ZrTiO}_4$  was yielded at 0.5%. MCC-2 analysis at  $150^\circ\text{C}$  in deionised water reported a normalised mass loss of Nd between  $10^{-3}$  and  $10^{-4}$  over 80 d. Single phase zirconolite doped with 0.15 f.u. of Nd (trivalent actinide surrogate) were recently fabricated by Cai et al. Subsequent to confirmation of a single product in the  $\text{Ca}_{1-x}\text{Zr}_{1-x}\text{Gd}_{2x}\text{Ti}_2\text{O}_7$  system, the sample with nominal composition  $\text{Ca}_{0.925}\text{Zr}_{0.925}\text{Gd}_{0.15}\text{Ti}_2\text{O}_7$  was selected for PCT analysis. The durability was measured in pH 5, 7, and 9 at  $90^\circ\text{C}$ . The single phase specimen demonstrated a normalised Nd leach rate of  $3.13 \times 10^{-5} \text{ gm}^{-2}\cdot\text{d}^{-1}$  after 42 d, proving insensitive to extraction under varying pH [137]. Recent work by Zhang et al. utilised  $\text{Gd}^{3+}$  and  $\text{Hf}^{4+}$  as trivalent and tetravalent actinide surrogates, with a view to eliminate the issues typically caused by Ce reduction, targeting the composition  $\text{Ca}_{1-x}\text{Hf}_{1-x}\text{Gd}_{2x}\text{Ti}_2\text{O}_7$  [138]. Release rates of  $4.72 \times 10^{-7}$  and  $1.59 \times 10^{-8} \text{ gm}^{-2}\cdot\text{d}^{-1}$  were measured for Gd and Hf respectively.

### Critical gap analysis

Zirconolite-rich wasteforms satisfy many of the design criteria commonly applied in the design of nuclear wasteform materials, not least high chemical durability and moderate wasteloading. Nevertheless, an in-depth review of the literature has identified several gaps that have not been conclusively addressed:

- **Polytype formation:** It has been demonstrated that the choice of substitution scheme, surrogate and thermal processing route are controlling factors in the formation of crystallographically distinct zirconolite polytype structures. However, although the acceptance criteria do not stipulate the preferred formation of a specific polytype, it has not been determined whether the formation of any specific zirconolite structure (i.e. 2M, 3T) will result in improved performance in the disposal environment.
- **Charge compensation species:** The incorporation of high valence cation (e.g.  $\text{Ce}^{4+}/\text{U}^{6+}$ ) within the  $\text{Ca}^{2+}$  site in zirconolite can be achieved by the accommodation of a lower valence cation within the  $\text{Ti}^{4+}$  site in a ratio sufficient to offset any apparent excess charge. A host of charge compensation species have been utilised in various studies,

including  $\text{Mg}^{2+}$ ,  $\text{Al}^{3+}$ ,  $\text{Fe}^{3+}$ , and  $\text{Nb}^{5+}$ . There is a need for a systematic evaluation as to whether any of these charge compensation species may afford increased durability relative to one another.

- **The use of chemical surrogates:** It has been highlighted that the use of chemical surrogates is necessary the development of wasteforms for actinides. Nevertheless, no surrogate species can sufficiently reproduce the chemical and physical properties required to reproduce Pu behaviour to a satisfactory level. The problems associated with Ce have been highlighted, and the tendency of Ce to undergo auto-reduction to  $\text{Ce}^{3+}$  at high temperatures has been demonstrated to promote the formation of undesirable secondary phases such as perovskite, making the elicitation of Ce release rates from the zirconolite phase difficult. The use of surrogates across the literature is typically limited to the use of a single analogous species, it is therefore necessary to use several surrogates in conjunction to allow a suite of behaviours analogous to Pu to be evaluated. As Pu exhibits a range of oxidation states, a multi-surrogate approach should be undertaken, with elements displaying a strong preference for (III) and (IV) oxidation states, that are relatively insensitive to imposed redox conditions. Furthermore, a detailed, systematic investigation of surrogates in the zirconolite system is necessary to support the safety case for geological disposal.
- **Processing methods:** Zirconolite is relatively unstable under reducing conditions, often resulting in the formation of parasitic perovskite phases that are determined to reduce the overall chemical durability of the wasteform. When assessing the durability of zirconolite compositions, variations in atmospheric processing conditions, synthesis temperature, and synthesis route (e.g. cold sintering, hot pressing, hot isostatic pressing) must be taken into consideration. As a result, it is difficult meaningful comparisons between data published regarding the synthesis and aqueous durability of zirconolite wasteforms for Pu immobilisation.

## Conclusions

The zirconolite wasteform is currently a candidate host phase for Pu, should U.K. Government policy adopt a strategy of immobilisation and disposal of the bulk inventory. Zirconolite chemistry permits the acceptance of a wide variety of REE<sup>3+</sup>/Ac<sup>4+</sup> ( $\text{U}^{4+}$ ,  $\text{Pu}^{3+/4+}$ ,  $\text{Th}^{4+}$ ,  $\text{Ce}^{3+/4+}$ ,  $\text{Sm}^{3+}$ ) within solid solution, alongside a considerable selection of charge balancing species ( $\text{Al}^{3+}$ ,  $\text{Mg}^{2+}$ ,  $\text{Fe}^{3+}$ ,  $\text{Nb}^{5+}$ ) for the formation of heterovalent compositions, and neutron poison species ( $\text{Gd}^{3+}$ ,  $\text{Hf}^{4+}$ ). A review of the literature has

identified that the incorporation of  $\text{Pu}^{4+}$  may be best achieved by homovalent substitution for  $\text{Zr}^{4+}$ , and/or heterovalent substitution for  $\text{Ca}^{2+}$ , with the addition of a suitable charge balancing species such as  $\text{Al}^{3+}$  or  $\text{Mg}^{2+}$ . In the case of the former mechanism, the substitution would likely be facilitated by the formation of the polytypical zirconolite-4M structure above 0.15 f.u.  $\text{Pu}^{4+}$ , a hybrid intergrowth between the nominal  $\text{CaZrTi}_2\text{O}_7$  aristotype and the  $\text{CaPuTi}_2\text{O}_7$  pyrochlore-structured phase. However, it is apparent that the 2M polytype may be stabilised over a wider solid solution range when favouring substitution for  $\text{Ca}^{2+}$ , with appropriate charge compensation. The formation of deleterious secondary phases such as perovskite is shown to be dependent on the method of substitution utilised and the valence of the surrogate element, which is in turn is controlled by processing conditions rather than crystallographic design. A survey of the literature confirms zirconolite exhibits exceptional chemical durability with normalised release rates for constituent elements typically of the order  $10^{-5}$  to  $10^{-8} \text{ gm}^{-2}\cdot\text{d}^{-1}$  under simulated disposal conditions.

## Acknowledgements

We acknowledge financial support from the Nuclear Decommissioning Authority (NDA) and EPSRC under grant numbers EP/S01019X/1, EP/S011935/1, EP/S020659/1, EP/P013600/1 and EP/R511754/1. This research utilised the HADES/MIDAS facility at the University of Sheffield established with financial support from EPSRC and BEIS [139].

## Disclosure statement

No potential conflict of interest was reported by the author (s).

## Funding

We acknowledge financial support from the Nuclear Decommissioning Authority (NDA) and EPSRC under grant numbers EP/S01019X/1, EP/S011935/1, EP/S020659/1, EP/P013600/1 and EP/R511754/1.

## ORCID

Lewis R. Blackburn  <http://orcid.org/0000-0002-5889-2035>

Laura J. Gardner  <http://orcid.org/0000-0003-3126-2583>

Neil C. Hyatt  <http://orcid.org/0000-0002-2491-3897>

## References

- [1] Donald IW. Waste immobilization in glass and ceramic based hosts. Chichester: Wiley; 2010.
- [2] Ojovan MI, Lee WE. An Introduction to nuclear waste immobilisation. 1st ed. Oxford: Elsevier; 2005.

- [3] Oh Chang H. Hazardous and radioactive waste treatment technologies handbook. Boca Raton: CRC Press; 2001.
- [4] Ojovan MI, Batyukhnova OG. Glasses for nuclear waste immobilization, In WM '07 Conference, Tuscon, AZ. 2007. p. 15.
- [5] Lopez C, Deschanel X, Den Auwer C, et al. X-ray absorption studies of borosilicate glasses containing dissolved actinides or surrogates. *Phys Scr.* 2005; T115:342–345.
- [6] Cachia J, Deschanel X, Den Auwer C, et al. Enhancing cerium and plutonium solubility by reduction in borosilicate glass. *J Nucl Mater.* 2006;352:182–189. doi:10.1016/j.jnucmat.2006.02.052.
- [7] Lopez C, Deschanel X, Bart JM, et al. Solubility of plutonium surrogates in nuclear glasses. In Scientific Research on the Back-End of the Fuel Cycle for the 21. Century, Avignon, France. 2000. p. 1–5.
- [8] Wellman DM, Icenhower JP, Weber WJ. Elemental dissolution study of Pu-bearing borosilicate glasses. *J Nucl Mater.* 2005;340:149–162. doi:10.1016/j.jnucmat.2004.10.166.
- [9] Lutze W, Ewing RC. Radioactive wastefoms for the future. Amsterdam: North Holland Physics Publishing; 1988.
- [10] Corkhill CL, Hyatt NC. Nuclear waste management. Bristol, UK: IOP Publishing; 2018.
- [11] McMaster SA, Ram R, Faris N, et al. Radionuclide disposal using the pyrochlore supergroup of minerals as a host matrix – a review. *J Hazard Mater.* 2018;360:257–269. doi:10.1016/j.jhazmat.2018.08.037.
- [12] Harrison MT, Scales CR. Durability of borosilicate glass compositions for the immobilisation of the UK's separated plutonium stocks. *Mater Res Soc Symp Proc.* Pittsburgh, PA. 2008;1107.
- [13] Lee WE, Ojovan MI, Stennett MC, et al. Immobilisation of radioactive waste in glasses, glass composite materials and ceramics. *Adv Appl Ceram.* 2006;105(1):3–12. doi:10.1179/174367606X81669.
- [14] Ewing RC. Ceramic matrices for plutonium disposition. *Prog Nucl Energy.* 2007;49:635–643. doi:10.1016/j.pnucene.2007.02.003.
- [15] Ewing RC. Nuclear waste forms for actinides. *Proc Natl Acad Sci USA.* 1999;96:3432–3439. doi:10.1073/pnas.96.7.3432.
- [16] Wang L, Liang T. Ceramics for high level radioactive waste solidification. *J Adv Ceram.* 2012;1(3):194–203. doi:10.1007/s40145-012-0019-8.
- [17] Weber WJ, Navrotsky A, Stefanovsky S, et al. Materials Science of high-level Immobilization. *MRS Bull.* 2009;34(01):46–52.
- [18] Stewart M, Begg B, Day R, et al. Low-risk alternative waste forms for actinide immobilization. In WM'05 Conference, Tuscon, AZ. 2004.
- [19] Gray LW, Kan T, Mckibbert JM. Immobilization as a route to surplus fissile materials disposition, vol. UCRL-JC-1, Lansdowne, VA. 1996.
- [20] Burakov BE, Ojovan MI, Lee WE. Crystalline materials for actinide immobilisation. 1st ed. London, UK: Imperial College Press; 2011.
- [21] Lumpkin GR. Ceramic waste forms for actinides. *Elements.* 2006;2(6):365–372. doi:10.2113/gselements.2.6.365.
- [22] Orlova AI, Ojovan MI. Ceramic mineral waste-forms for nuclear waste immobilization. *Materials (Basel).* 2019;12(16):2638. doi:10.3390/ma12162638.
- [23] Hart KP, Zhang Y, Loi E, et al. Aqueous durability of titanate ceramics designed to immobilise excess plutonium. *Mat Res Soc Symp Proc.* 2000;608:353–358.
- [24] Vance ER, Agrawal DK. Incorporation of radionuclides in crystalline titanates. *Nucl Chem Waste Manag.* 1982;3(4):229–234. doi:10.1016/0191-815X(82)90004-3.
- [25] Strachan DM, Scheele RD, Buck EC, et al. Radiation damage effects in candidate titanates for Pu disposition: zirconolite. *J Nucl Mater.* 2008;372(1):16–31. doi:10.1016/j.jnucmat.2007.01.278.
- [26] Vance ER, Angel PJ, Begg BD, et al. Zirconolite-rich titanate ceramics for high-level actinide wastes. *Mat Res Soc Symp Proc.* 1994;333:293–298.
- [27] Zhang FX, Manoun B, Saxena SK. Pressure-induced order-disorder transitions in pyrochlore RE<sub>2</sub>Ti<sub>2</sub>O<sub>7</sub> (RE = Y, Gd). *Mater Lett.* 2006;60(21–22):2773–2776. doi:10.1016/j.matlet.2006.01.095.
- [28] Kong L, Zhang Y, Karatchevtseva I. Preparation of Y<sub>2</sub>Ti<sub>2</sub>O<sub>7</sub> pyrochlore glass-ceramics as potential waste forms for actinides: the effects of processing conditions. *J Nucl Mater.* 2017;494:29–36. doi:10.1016/j.jnucmat.2017.07.004.
- [29] Wei T, Zhang Y, Kong L, et al. Hot isostatically pressed Y<sub>2</sub>Ti<sub>2</sub>O<sub>7</sub> and Gd<sub>2</sub>Ti<sub>2</sub>O<sub>7</sub> pyrochlore glass-ceramics as potential waste forms for actinide immobilization. *J Eur Ceram Soc.* 2019;39(4):1546–1554. doi:10.1016/j.jeurceramsoc.2018.11.012.
- [30] Lang M, Zhang F, Zhang J, et al. Review of A<sub>2</sub>B<sub>2</sub>O<sub>7</sub> pyrochlore response to irradiation and pressure. *Nucl Instrum Methods Phys Res B: Beam Interact Mater At.* 2010;268(19):2951–2959. doi:10.1016/j.nimb.2010.05.016.
- [31] Cleave A, Grimes RW, Sickafus K. Plutonium and uranium accommodation in pyrochlore oxides. *Philos Mag.* 2005;85(9):967–980. doi:10.1080/14786430412331314672.
- [32] Wang L, Xie H, Chen Q, et al. Study on the solubility of uranium in the pyrochlore lattice of Nd<sub>2</sub>Zr<sub>2</sub>O<sub>7</sub>. *Mater Sci.* 2015;5(4):184–190.
- [33] Lumpkin GR, Hart KP, McGlinn PJ, et al. Retention of actinides in natural pyrochlores and zirconolites. *Radiochim Acta.* 1994;66/67:469–474.
- [34] Zhang Y, Li H, Moricca S. Pyrochlore-structured titanate ceramics for immobilisation of actinides: hot isostatic pressing (HIPing) and stainless steel/waste form interactions. *J Nucl Mater.* 2008;377:470–475. doi:10.1016/j.jnucmat.2008.03.022.
- [35] McMaster SA, Ram R, Charalambous F, et al. Synthesis and characterisation of the uranium pyrochlore betafite [(Ca,U)<sub>2</sub>(Ti,Nb,Ta)<sub>2</sub>O<sub>7</sub>]. *J Hazard Mater.* 2014;280:478–486. doi:10.1016/j.jhazmat.2014.07.062.
- [36] Ewing RC, Weber WJ, Lian J. Nuclear waste disposal-pyrochlore (A<sub>2</sub>B<sub>2</sub>O<sub>7</sub>): nuclear waste form for the immobilization of plutonium and 'minor' actinides. *J Appl Phys.* 2004;95(11):5949–5971. doi:10.1063/1.1707213.
- [37] Ewing RC, Lutze W. Zircon: a host-phase for the disposal of weapons plutonium. *J Mater Res.* 1995;10(2):243–246. doi:10.1557/JMR.1995.0243.
- [38] Cherniak DJ. Diffusion of helium in radiation-damaged zircon. *Chem Geol.* 2019;529. doi:10.1016/j.chemgeo.2019.119308.

- [39] Ding Y, Lu X, Dan H, et al. Phase evolution and chemical durability of Nd-doped zircon ceramics designed to immobilize trivalent actinides. *Ceram Int.* 2015;41(8):10044–10050. doi:10.1016/j.ceramint.2015.04.092.
- [40] Xie Y, Fan L, Shu X, et al. Chemical stability of Ce-doped zircon ceramics: influence of pH, temperature and their coupling effects. *J Rare Earths.* 2017;35(2):164–171. doi:10.1016/S1002-0721(17)60895-0.
- [41] Horie K, Hidaka H, Gauthier-Lafaye F. Elemental distribution in apatite, titanite and zircon during hydrothermal alteration: durability of immobilization mineral phases for actinides. *Phys Chem Earth.* 2008;33(14–16):962–968. doi:10.1016/j.pce.2008.05.008.
- [42] Trocellier P, Delmas R. Chemical durability of zircon. *Nucl Instrum Methods Phys Res B: Beam Interact Mater At.* 2001;181:408–412. doi:10.1016/S0168-583X(01)00377-9.
- [43] Thomé L, Gentils A, Jagielski J, et al. Radiation stability of ceramics: test cases of zirconia and spinel. *Vacuum.* 2007;81(10):1264–1270. doi:10.1016/j.vacuum.2007.01.021.
- [44] Yu N, Sickafus KE, Kodali P, et al. In situ observation of defect growth beyond the irradiated region in yttria-stabilized zirconia induced by 400 keV xenon ion-beam at  $-90$  and  $30^{\circ}\text{C}$ . *J Nucl Mater.* 1997;244:266–272.
- [45] Yasuda K, Kinoshita C, Matsumura S, et al. Radiation-induced defect clusters in fully stabilized zirconia irradiated with ions and/or electrons. *J Nucl Mater.* 2003;319:74–80. doi:10.1016/S0022-3115(03)00136-3.
- [46] Costantini JM, Beuneu F, Weber WJ. Radiation damage in cubic-stabilized zirconia. *J Nucl Mater.* 2013;440(1–3):508–514. doi:10.1016/j.jnucmat.2013.02.041.
- [47] Burakov BE, Yagovkina MA. A study of accelerated radiation damage effects in  $\text{PuO}_2$  and gadolinia-stabilized cubic zirconia,  $\text{Zr}_{0.79}\text{Gd}_{0.14}\text{Pu}_{0.07}\text{O}_{1.93}$ , doped with  $^{238}\text{Pu}$ . *J Nucl Mater.* 2015;467:534–536. doi:10.1016/j.jnucmat.2015.10.032.
- [48] Kulkarni NK, Sampath S, Venugopal V. Studies on stabilised zirconia as host phase for the fixation of actinides, rare-earths and sodium. *Ceram Int.* 2001;27(8):839–846. doi:10.1016/S0272-8842(01)00038-4.
- [49] Ding Y, Dan H, Lu X, et al. Phase evolution and chemical durability of  $\text{Zr}_{1-x}\text{Nd}_x\text{O}_{2-x/2}$  ( $0 \leq x \leq 1$ ) ceramics. *J Eur Ceram Soc.* 2017;37(7):2673–2678. doi:10.1016/j.jeurceramsoc.2017.02.053.
- [50] Gilbert M, Davoisne C, Stennett M, et al. Krypton and helium irradiation damage in neodymium-zirconolite. *J Nucl Mater.* Sep. 2011;416(1–2):221–224. doi:10.1016/J.JNUCMAT.2010.11.089.
- [51] Li W, Dong F, Bian L, et al. Phase relations, microstructure, and valence transition studies on  $\text{CaZr}_{1-x}\text{Ce}_x\text{Ti}_2\text{O}_7$  ( $0.0 \leq x \leq 1.0$ ) system. *J Rare Earths.* 2018;36(11):1184–1189. doi:10.1016/j.jre.2018.04.006.
- [52] Gatehouse BM, Grey IE, Hill RJ, et al. Zirconolite,  $\text{CaZr}_x\text{Ti}_{3-x}\text{O}_7$ ; structure refinements for near-end-member compositions with  $x = 0.85$  and  $1.30$ . *Acta Cryst.* 1981;B37(1974):306–312. doi:10.1107/S0567740881002914.
- [53] Deschanel X, Broudic V, Jegou C, et al. Pu-doped zirconolite for minor actinide containment. *ATALANTE.* 2004;2004:1–6.
- [54] Bohre A, Avasthi K, Shrivastava OP. Synthesis, characterization, and crystal structure refinement of lanthanum and yttrium substituted polycrystalline 2M type zirconolite phases:  $\text{Ca}_{1-x}\text{M}_x\text{ZrTi}_2\text{O}_7$  ( $\text{M} = \text{Y}, \text{La}$  and  $x = 0.2$ ). *J Powder Technol.* 2014;2014:1–10. doi:10.1155/2014/902317.
- [55] Vance ER, Lumpkin GR, Carter ML, et al. Incorporation of uranium in zirconolite ( $\text{CaZrTi}_2\text{O}_7$ ). *J Am Ceram Soc.* 2002;85(7):1853–1859. doi:10.1111/j.1151-2916.2002.tb00364.x.
- [56] Clark BM, Sundaram SK, Misture ST. Polymorphic transitions in cerium-substituted zirconolite ( $\text{CaZrTi}_2\text{O}_7$ ). *Sci Rep.* 2017;7(1):2–10. doi:10.1038/s41598-017-06407-5.
- [57] Caurant D, Loiseau P, Bardez I. Structural characterization of Nd-doped Hf-zirconolite  $\text{Ca}_{1-x}\text{Nd}_x\text{HfTi}_{2-x}\text{Al}_x\text{O}_7$  ceramics. *J Nucl Mater.* 2010;407(2):88–99. doi:10.1016/j.jnucmat.2010.09.033.
- [58] Salamat A, McMillan PF, Firth S, et al. Structural transformations and disordering in zirconolite ( $\text{CaZrTi}_2\text{O}_7$ ) at high pressure. *Inorg Chem.* 2013;52:1550–1558. doi:10.1021/ic302346g.
- [59] Hyatt NC, Stennett MC, Maddrell ER, et al. Single phase ceramic wasteforms for plutonium disposition. *Adv Sci Technol.* 2006;45(2006):2004–2011. doi:10.4028/www.scientific.net/ast.45.2004.
- [60] Thornber S, Stennett MC, Hyatt NC. Investigation of Ce incorporation in zirconolite glass-ceramics for UK plutonium disposition. In 2016 MRS Fall Meeting, Boston, MA. 2016.
- [61] Bailey DJ, Lawson SM, Sun SK, et al. A new approach to the immobilisation of technetium and transuranics: Co-disposal in a zirconolite ceramic matrix. *J Nucl Mater.* 2019;528:151885, doi:10.1016/j.jnucmat.2019.151885.
- [62] Sun S-K, Stennett MC, Corkhill CL, et al. Reactive spark plasma synthesis of  $\text{CaZrTi}_2\text{O}_7$  zirconolite ceramics for plutonium disposition. *J Nucl Mater.* 2018 Mar;500:11–14. doi:10.1016/J.JNUCMAT.2017.12.021.
- [63] Kong L, Karatchevtseva I, Chironi I, et al.  $\text{CaZrTi}_2\text{O}_7$  zirconolite synthesis: from ceramic to glass-ceramic. *Int J Appl Ceram Technol.* 2019;16(4):1460–1470. doi:10.1111/ijac.13203.
- [64] Ma S, Ji S, Liao C, et al. Effects of ionic radius on phase evolution in Ln-Al co-doped  $\text{Ca}_{1-x}\text{Ln}_x\text{ZrTi}_{2-x}\text{Al}_x\text{O}_7$  ( $\text{Ln} = \text{La}, \text{Nd}, \text{Gd}, \text{Ho}, \text{Yb}$ ) solid solutions. *Ceram Int.* 2018;44(13):15124–15132. doi:10.1016/j.ceramint.2018.05.149.
- [65] Arinicheva Y, Gausse C, Neumeier S, et al. Influence of temperature on the dissolution kinetics of synthetic  $\text{LaPO}_4$ -monazite in acidic media between  $50$  and  $130^{\circ}\text{C}$ . *J Nucl Mater.* 2018;509:488–495. doi:10.1016/j.jnucmat.2018.07.009.
- [66] Meng C, Ding X, Zhao J, et al. Preparation and characterization of cerium-gadolinium monazites as ceramics for the conditioning of minor actinides. *Prog Nucl Energy.* 2016;89:1–6. doi:10.1016/j.pnucene.2016.01.021.
- [67] Schlenz H, Dellen J, Kegler P, et al. Structural and thermodynamic mixing properties of  $\text{La}_{1-x}\text{Nd}_x\text{PO}_4$  monazite-type solid solutions. *J. Solid State Chem.* 2019;270(November 2018):470–478. doi:10.1016/j.jssc.2018.11.040.
- [68] Rawat D, Phapale S, Mishra R, et al. Thermodynamic investigation of thorium and strontium substituted monazite solid-solution. *Thermochim Acta.*

- 2019;674(April 2018):10–20. doi:10.1016/j.tca.2019.01.031.
- [69] Brandt F, Neumeier S, Schuppik T, et al. Conditioning of minor actinides in lanthanum monazite ceramics: a surrogate study with europium. *Prog Nucl Energy*. 2014;72:140–143. doi:10.1016/j.pnucene.2013.07.019.
- [70] Heuser J, Bukaemskiy AA, Neumeier S, et al. Raman and infrared spectroscopy of monazite-type ceramics used for nuclear waste conditioning. *Prog Nucl Energy*. 2014;72:149–155. doi:10.1016/j.pnucene.2013.09.003.
- [71] Gausse C, Szenknect S, Mesbah A, et al. Dissolution kinetics of monazite  $\text{LnPO}_4$  (Ln = La to Gd): a multi-parametric study. *Appl Geochemistry*. 2018;93 (April):81–93. doi:10.1016/j.apgeochem.2018.04.005.
- [72] Zhao X, Li Y, Teng Y, et al. The effect of Ce content on structure and stability of  $\text{Gd}_{1-x}\text{Ce}_x\text{PO}_4$ : theory and experiment. *J Eur Ceram Soc*. 2019;39(4):1555–1563. doi:10.1016/j.jeurceramsoc.2018.11.009.
- [73] Clavier N, Mesbah A, Szenknect S, et al. Monazite, rhabdophane, xenotime & churchite: vibrational spectroscopy of gadolinium phosphate polymorphs. *Spectrochim Acta A: Mol Biomol Spectrosc*. 2018;205:85–94. doi:10.1016/j.saa.2018.07.016.
- [74] Zhao X, Li Y, Teng Y, et al. The structure properties, defect stability and excess properties in Am-doped  $\text{LnPO}_4$  (Ln = La, Ce, Nd, Sm, Eu, Gd) monazites. *J Alloys Compd*. 2019;806:113–119. doi:10.1016/j.jallcom.2019.07.251.
- [75] Proust V, Jeannin R, White FD, et al. Tailored perovskite waste forms for plutonium trapping. *Inorg Chem*. 2019;58(5):3026–3032. doi:10.1021/acs.inorgchem.8b02832.
- [76] Kastrissos T, Stephenson M, Turner P, et al. Hydrothermal dissolution of perovskite ( $\text{CaTiO}_3$ ): implications for synroc formulation. *J Am Ceram Soc*. 1987;70(7):144–146. doi:10.1007/BF01161185.
- [77] Davoisne C, Stennett MC, Hyatt NC, et al. Krypton irradiation damage in Nd-doped zirconolite and perovskite. *J Nucl Mater*. 2011;415(1):67–73. doi:10.1016/j.jnucmat.2011.05.043.
- [78] Begg B, Vance E, Conradson S. The incorporation of plutonium and neptunium in zirconolite and perovskite. *J Alloys Compd*. 1998;271–273:221–226. doi:10.1016/S0925-8388(98)00058-9.
- [79] Begg BD, Zhang Y, Vance ER, et al. Effect of Pu valence on acid dissolution of perovskite ( $\text{CaTiO}_3$ ). *AIP Conf Proc*. 2003;673:131–132. doi:10.1063/1.1594577.
- [80] Begg BD, Vance ER, Lumpkin GR. Charge compensation and the incorporation of cerium in zirconolite and perovskite. *Mat Res Soc Symp Proc*. 1998;506:79–86. doi:10.1557/PROC-506-79.
- [81] Pham DK, Neall FB, Myhra S, et al. Dissolution mechanisms of  $\text{CaTiO}_3$  – solution analysis, surface analysis and electron microscope studies – implications for synroc. *Mat Res Soc Symp Proc*. 1989;127:231–240.
- [82] Zhang Y, Karatchevseva I, Qin M, et al. Raman spectroscopic study of natural and synthetic brannerite. *J Nucl Mater*. 2013;437(1–3):149–153. doi:10.1016/j.jnucmat.2013.02.004.
- [83] Zhang Y, Lumpkin GR, Li H, et al. Recrystallisation of amorphous natural brannerite through annealing: the effect of radiation damage on the chemical durability of brannerite. *J Nucl Mater*. 2006;350(3):293–300. doi:10.1016/j.jnucmat.2006.01.012.
- [84] Zhang Y, Thomas BS, Lumpkin GR, et al. Dissolution of synthetic brannerite in acidic and alkaline fluids. *J Nucl Mater*. 2003;321(1):1–7. doi:10.1016/S0022-3115(03)00203-4.
- [85] Stennett MC, Freeman CL, Gandy AS, et al. Crystal structure and non-stoichiometry of cerium brannerite:  $\text{Ce}_{0.975}\text{Ti}_2\text{O}_{5.95}$ . *J Solid State Chem*. 2012;192:172–178. doi:10.1016/j.jssc.2012.03.057.
- [86] James M, Carter ML, Watson JN. The synthesis, crystal chemistry and structures of Y-doped brannerite ( $\text{U}_{1-x}\text{Y}_x\text{Ti}_2\text{O}_6$ ) and thorutite ( $\text{Th}_{1-x}\text{Y}_x\text{Ti}_2\text{O}_{6-\delta}$ ) phases. *J Solid State Chem*. 2003;174(2):329–333. doi:10.1016/S0022-4596(03)00230-5.
- [87] Bailey DJ, Stennett MC, Ravel B, et al. Synthesis and characterisation of brannerite compositions ( $\text{U}_{0.9}\text{Ce}_{0.1}$ ) $_{1-x}\text{M}_x\text{Ti}_2\text{O}_6$  (M =  $\text{Gd}^{3+}$ ,  $\text{Ca}^{2+}$ ) for the immobilisation of MOX residues. *RSC Adv*. 2018;8 (4):2092–2099. doi:10.1039/C7RA11742F.
- [88] Valeš V, Matějová L, Matěj Z, et al. Crystallization kinetics study of cerium titanate  $\text{CeTi}_2\text{O}_6$ . *J Phys Chem Solids*. 2014;75(2):265–270. doi:10.1016/j.jpcs.2013.10.001.
- [89] Gilligan R, Nikoloski AN. The extraction of uranium from brannerite – a literature review. *Miner Eng*. 2015;71:34–48. doi:10.1016/j.mineng.2014.10.007.
- [90] Lumpkin GR, Leung SHF, Ferenczy J. Chemistry, microstructure, and alpha decay damage of natural brannerite. *Chem Geol*. 2012;291:55–68. doi:10.1016/j.chemgeo.2011.09.008.
- [91] Lumpkin GR, Gao Y, Gieré R, et al. The role of Th-U minerals in assessing the performance of nuclear waste forms. *Mineral Mag*. 2014;78(5):1071–1095. doi:10.1180/minmag.2014.078.5.01.
- [92] Williams CT, Gieré R. Zirconolite: a review of Localities worldwide, and a compilation of its chemical compositions. *Bull Nat Hist Museum London*. 1996;52:1–24.
- [93] Hart KP, Lumpkin GR, Gieré R, et al. Naturally-occurring zirconolites – analogues for the long-term encapsulation of actinides in synroc. *Radiochim Acta*. 1996;74:309–312. doi:10.1524/ract.1996.74.special-issue.309.
- [94] Lumpkin GR. Alpha-decay damage and aqueous durability of actinide host phases in natural systems. *J Nucl Mater*. 2001;289(1–2):136–166. doi:10.1016/S0022-3115(00)00693-0.
- [95] McCauley RA, Hummel FA. New pyrochlores of the charge-coupled type. *J Solid State Chem*. 1980;33(1):99–105. doi:10.1016/0022-4596(80)90552-6.
- [96] Farmer JM, Boatner LA, Chakoumakos BC, et al. Structural and crystal chemical properties of rare-earth titanate pyrochlores. *J Alloys Compd*. 2014;605:63–70. doi:10.1016/j.jallcom.2014.03.153.
- [97] Vance ER, Jostons A, Day RA, et al. Excess Pu disposition in zirconolite-rich synroc. *Mat Res Soc Symp Proc*. 1996;412:41–47.
- [98] Kesson SE, Sinclair WJ, Ringwood AE. Solid solution limits in synroc zirconolite. *Nucl Chem Waste Manag*. 1983;4:259–265.
- [99] Buck EC, Ebbinghaus B, Bakel AJ, et al. Characterization of a Pu-bearing zirconolite-rich synroc. In *MRS Fall Meeting, Boston, MA*. 1996.
- [100] Smith KL, Lumpkin GR, Blackford MG, et al. Characterization and leaching behavior of plutonium-bearing synroc-C. *Mat Res Soc Symp Proc*. 1997;465:1267–1272.

- [101] White TJ, Segall RL, Hutchison JL, et al. Polytropic behaviour of zirconolite. *Proc R Soc Lond A*. 1984;392:343–358. doi:10.1098/rspa.1936.0060.
- [102] Cheary RW, Coelho AA. A site occupancy analysis of zirconolite  $\text{CaZr}_x\text{Ti}_{3-x}\text{O}_7$ . *Phys Chem Miner*. 1997;24:447–454.
- [103] Coelho AA, Cheary RW, Smith KL. Analysis and structural determination of Nd-substituted zirconolite-4M. *J Solid State Chem*. 1997;129:346–359. doi:10.1006/jssc.1996.7263.
- [104] Gilbert MR, Selfslag C, Walter M, et al. Synthesis and characterisation of Pu-doped zirconolites –  $(\text{Ca}_{1-x}\text{Pu}_x)\text{Zr}(\text{Ti}_{2-2x}\text{Fe}_{2x})\text{O}_7$ . *IOP Conf Ser Mater Sci Eng*. 2010;9(012007): doi:10.1088/1757-899X/9/1/012007.
- [105] Begg BD, Day RA, Brownscombe A. Structural effect of Pu substitutions on the Zr-site in zirconolite. *Mat Res Soc Symp Proc*. 2001;663:1–8.
- [106] Vance ER, Begg BD, Day RA, et al. Zirconolite-rich ceramics for actinide wastes. *Mat Res Soc Symp Proc*. 1995;353:767–774.
- [107] Rossell HJ. Solid solution of metal oxides in the zirconolite phase  $\text{CaZrTi}_2\text{O}_7$ . II: the ternary phase  $\text{CaZr}_x\text{Ti}_{3-x}\text{O}_7$ . *J. Solid State Chem*. 1992;99(1):52–57. doi:10.1016/0022-4596(92)90287-6.
- [108] Liao CZ, Shih K, Lee WE. Crystal structures of Al-Nd Codoped zirconolite derived from glass matrix and powder sintering. *Inorg Chem*. 2015;54(15):7353–7361. doi:10.1021/acs.inorgchem.5b00847.
- [109] Whittle KR, Hyatt NC, Smith KL, et al. Combined neutron and X-ray diffraction determination of disorder in doped zirconolite-2M. *Am Mineral*. 2012;97:291–298.
- [110] Jafar M, Achary SN, Salke NP, et al. X-ray diffraction and Raman spectroscopic investigations on  $\text{CaZrTi}_2\text{O}_7 - \text{Y}_2\text{Ti}_2\text{O}_7$  system: delineation of phase fields consisting of potential ceramic host materials. *J Nucl Mater*. 2016;475:192–199. doi:10.1016/j.jnucmat.2016.04.016.
- [111] Jafar M, Sengupta P, Achary SN, et al. Phase evolution and microstructural studies in  $\text{CaZrTi}_2\text{O}_7 - \text{Nd}_2\text{Ti}_2\text{O}_7$  system. *J Am Ceram Soc*. 2014;97(2):609–616. doi:10.1111/jace.12664.
- [112] Jafar M, Sengupta P, Achary SN, et al. Phase evolution and microstructural studies in  $\text{CaZrTi}_2\text{O}_7$  (zirconolite)- $\text{Sm}_2\text{Ti}_2\text{O}_7$  (pyrochlore) system. *J Eur Ceram Soc*. 2014;34(16):4373–4381. doi:10.1016/j.jeurceramsoc.2014.07.001.
- [113] Zhang YB, Wang J, Wang JX, et al. Phase evolution, microstructure and chemical stability of  $\text{Ca}_{1-x}\text{Zr}_{1-x}\text{Gd}_x\text{Ti}_2\text{O}_7$  ( $0.0 \leq x \leq 1.0$ ) system for immobilizing nuclear waste. *Ceram Int*. 2018;44(12):13572–13579. doi:10.1016/j.ceramint.2018.04.191.
- [114] Begg BD, Vance ER. The incorporation of cerium in zirconolite. *Mat Res Soc Symp Proc*. 1997;465:333–340.
- [115] Blackburn LR, Sun S, Gardner LJ, et al. A systematic investigation of the phase assemblage and microstructure of the zirconolite  $\text{CaZr}_{1-x}\text{Ce}_x\text{Ti}_2\text{O}_7$  system. *J Nucl Mater*. 2020;535:152137. doi:10.1016/j.jnucmat.2020.152137.
- [116] Blackburn LR, Gardner LJ, Sun SK, et al. Hot Isostatically pressed zirconolite wastefoms for actinide immobilisation. *IOP Conf Ser: Mater Sci Eng*. 2020. doi:10.1088/1757-899X/818/1/012010.
- [117] Vance ER, Ball CJ, Day RA, et al. Actinide and rare earth incorporation into zirconolite. *J Alloys Compd*. 1994;213/214:406–409. doi:10.1016/0925-8388(94)90945-8.
- [118] Kaur R, Gupta M, Kulriya PK, et al. Phase analysis and reduction behaviour of Ce dopant in zirconolite. *J Radioanal Nucl Chem*. 2019 Mar. doi:10.1007/s10967-019-06536-3.
- [119] Pöml P, Geisler T, Cobos-Sabaté J, et al. The mechanism of the hydrothermal alteration of cerium- and plutonium-doped zirconolite. *J Nucl Mater*. 2011;410(1–3):10–23. doi:10.1016/j.jnucmat.2010.12.218.
- [120] Blackburn LR, Sun S, Lawson SM, et al. Synthesis and characterisation of  $\text{Ca}_{1-x}\text{Ce}_x\text{ZrTi}_{2-2x}\text{Cr}_{2x}\text{O}_7$ : analogue zirconolite wasteform for the immobilisation of Stockpiled UK plutonium. *J Eur Ceram Soc*. 2020;40(15):5909–5919. doi:10.1016/j.jeurceramsoc.2020.05.066.
- [121] Lumpkin GR, Smith KL, Blackford MG. Partitioning of uranium and rare earth elements in synroc: effect of impurities, metal additive, and waste loading. *J Nucl Mater*. 1995;224(1):31–42. doi:10.1016/0022-3115(95)00037-2.
- [122] Ringwood AE, Oversby VM, Kesson SE, et al. Immobilization of high-level nuclear reactor wastes in synroc: a current appraisal. *Nucl Waste Manag*. 1981;2:287–305.
- [123] Zhang Y, Stewart MWA, Li H, et al. Zirconolite-rich titanate ceramics for immobilisation of actinides - waste form/HIP can interactions and chemical durability. *J Nucl Mater*. 2009;395:69–74. doi:10.1016/j.jnucmat.2009.09.019.
- [124] Li H, Zhang Y, McGlenn PJ, et al. Characterisation of stainless steel-synroc interactions under hot isostatic pressing (HIPing) conditions. *J Nucl Mater*. 2006;355(1–3):136–141. doi:10.1016/j.jnucmat.2006.05.014.
- [125] Dickson FJ, Hawkins KD, White TJ. Calcium uranium titanate – a new pyrochlore. *J Solid State Chem*. 1989;82(1):146–150. doi:10.1016/0022-4596(89)90234-X.
- [126] Shrivastava OP, Kumar N, Sharma IB. Synthesis, characterization and structural refinement of polycrystalline uranium substituted zirconolite  $\text{CaZr}_{0.9}\text{U}_{0.1}\text{Ti}_2\text{O}_7$ . *Radiochim Acta*. 2006;94(6–7):339–342. doi:10.1524/ract.2006.94.6.339.
- [127] Subramani T, Baker J, Xu H, et al. Synthesis, characterization, and enthalpies of formation of uranium substituted zirconolites. *ACS Earth Sp Chem*. 2020;4(10):1878–1887. doi:10.1021/acsearthspacechem.0c00182.
- [128] Begg BD, Vance ER, Day RA, et al. Plutonium and neptunium incorporation in zirconolite. *Mater Res Soc Symp – Proc*. 1997;465:325–332. doi:10.1557/proc-465-325.
- [129] Hyatt NC, Ojovan MI. Special issue: materials for nuclear waste immobilization. *Materials (Basel)*. 2019;12(21). doi:10.3390/ma12213611.
- [130] Oversby VA, Ringwood AE. Leach testing of synroc and glass samples at 85 and 200°C. *Nucl Chem. Waste Manag*. 1981;2:201–206.
- [131] Smith KL, Lumpkin GR, Blackford MG, et al. The durability of synroc. *J Nucl Mater*. 1992;190:287–294. doi:10.1016/0022-3115(92)90092-Y.
- [132] Zhang K, Yin D, Peng L, et al. Self-propagating synthesis and  $\text{CeO}_2$  immobilization of zirconolite-rich composites using  $\text{CuO}$  as the oxidant. *Ceram Int*. 2017;43:1415–1423. doi:10.1016/j.ceramint.2016.10.103.



- [133] Meng C, Ding X, Li W, et al. Phase structure evolution and chemical durability studies of Ce-doped zirconolite–pyrochlore synroc for radioactive waste storage. *J Mater Sci.* 2016;51:5207–5215. doi:10.1007/s10853-016-9822-x.
- [134] Wen G, Zhang K, Yin D, et al. Solid-state reaction synthesis and aqueous durability of Ce-doped zirconolite-rich ceramics. *J Nucl Mater.* 2015;466:113–119. doi:10.1016/j.jnucmat.2015.07.047.
- [135] Mcglinn PJ, Hart KP, Loi EH, et al. Ph dependence of the aqueous dissolution rates of perovskite and zirconolite at 90 °C. *Mat Res Soc Symp Proc.* 1995;353(3):847–854.
- [136] Zhang Z, Blackford MG, Lumpkin GR, et al. Aqueous dissolution of perovskite ( $\text{CaTiO}_3$ ): effects of surface damage and  $[\text{Ca}^{2+}]$  in the leachant. *J Mater Res.* 2005;20(9):2462–2473. doi:10.1557/JMR.2005.0294.
- [137] Cai X, Teng Y, Wu L, et al. The synthesis and chemical durability of Nd-doped single-phase zirconolite solid solutions. *J Nucl Mater.* 2016;479:455–460. doi:10.1016/j.jnucmat.2016.07.042.
- [138] Zhang K, Yin D, Xu K, et al. Self-propagating synthesis and characterization studies of Gd-bearing Hf-zirconolite ceramic waste forms. *Materials (Basel).* 2019;12(1), doi:10.3390/ma12010178.
- [139] Hyatt NC, Corkhill CL, Stennett MC, et al. The HADES facility for high activity decommissioning engineering & science: part of the UK National nuclear user facility. *IOP Conf Ser: Mater Sci Eng.* 2020;818:1–8. doi:10.1088/1757-899X/818/1/012022.